General Disclaimer

One or more of the Following Statements may affect this Document

- This document has been reproduced from the best copy furnished by the organizational source. It is being released in the interest of making available as much information as possible.

- This document may contain data, which exceeds the sheet parameters. It was furnished in this condition by the organizational source and is the best copy available.

- This document may contain tone-on-tone or color graphs, charts and/or pictures, which have been reproduced in black and white.

- This document is paginated as submitted by the original source.

- Portions of this document are not fully legible due to the historical nature of some of the material. However, it is the best reproduction available from the original submission.

Produced by the NASA Center for Aerospace Information (CASI)

08235-1-F

A Laboratory and Design Study of the Experiments for a Small Aeronomy Satellite

July 1968

Under contract with:

National Aeronautics and Space Administration
Contract No. NASr-54(13)
Washington, D.C.

High Altitude Engineering Laboratory
Department of Aerospace Engineering

N 69-22930

FACILITY FORM 602

(ACCESSION NUMBER) 103 (PAGES) CR-100586 (NASA CR OR TMX OR AD NUMBER)

(THRU) 1 (CODE) 14 (CATEGORY)

08235-1-F

THE UNIVERSITY OF MICHIGAN

COLLEGE OF ENGINEERING

Department of Aerospace Engineering
High Altitude Engineering Laboratory

Final Report

A LABORATORY AND DESIGN STUDY OF THE EXPERIMENTS FOR A SMALL AERONOMY SATEI ΓE

Under contract with:

National Aeronautics and Space Administration

Contract No. NASr-54(13)

Washington, D. C.

Administered through:

July 1968

OFFICE OF RESEARCH ADMINISTRATION ANN ARBOR

Project Personnel

Bonfanti, Giovanni, Assistant Research Engineer

Deakin, Lulu W., Secretary

Hays, Paul B., Assistant Professor, Aerospace Engineering

Jones, Leslie M., Professor, Aerospace Engineering

Marlatt, C. Ward, Administrative Associate

McWatters, Kenneth D., Research Associate

Schulte, Hal F., Research Engineer

Schumacher, Robert E., Assistant in Research

Wenzel, Elton A., Associate Research Engineer

Table of Contents

Final Report

A Laboratory and Design Study of the Experiments for a Small Aeronomy Satellite

Summary

This is the final report on Contract No. NASr-54(13) in which the aeronomy group in the Department of Aerospace Engineering at the University of Michigan addressed itself to several problems of designing the experiments and a satellite vehicle for making aeronomical measurements. For background material on the spacecraft mission please refer to a proposal and supplement for MICHAEL (Univ. of Mich. ORA-64 1237-PB1) submitted to NASA in April 1964 and April 1965 respectively. In the course of the work on the small satellite project several problems were identified. Among the most important were the behavior of a mass spectrometer oscillating slowly with respect tothe orbital path vector and the corallary question of whether or not the composition results obtained from spectrometers in this situation could be used to measure ambient temperature. The first section of the report is the result of that investigation.

A second important problem is the effect of outgassing and of gas-surface interactions of the input surfaces of mass spectrometers on the performance and errors of these instruments. An experimental approach to the problem was proposed which required the acquisition of a laboratory mass spectrometer and a modern vacuum system capable of 10^{-11} torr. The former device was provided by the College of Engineering and the latter purchased with NASA contract funds. The vacuum system is a Varian ion and sublimation pump with sorption cryogenic forepump. The stainless steel chamber has more than 50 liters capacity and is fitted with parts for observation, insertions and attachments. The combined spectrometer, pumping system and associated controls constitutes an eminently satisfactory basic system for the proposed work. During the contract

interval the apparatus was received, installed, and made operational. One section of the report is devoted to a description of the experiments and the special apparatus designed for the gas surface interaction studies. The actual investigations have only just started under the NASA sponsored Program in Aeronomy at Michigan and will be reported under Contract No. NASr-54(05). As part of the general work with mass spectrometers a low power ion source was developed and this also is briefly described.

A third key problem is to design the means by which the desired angles and motions between the spectrometer and the flight path vector are to be achieved. One part of the report is an analysis of the motion of a three body satellite under the action of gravitational and magnetic torques.

Two technique developments of considerable significance were undertaken with partial support from the subject contract. In the first instance three methods for measuring electron density were developed for possible use on a small satellite. These employed the measurement of transmission between two antennas, the impedance of a single antenna and the resonance relaxation of the ambient plasma. The methods were flown on Aerobee 4.207 VA on 8 August 1967 and all worked successfully. The results will be reported under Contract No. NASr-54(05) which supported the rocket flights. Theoretical work conducted by E. K. Miller and associated with the foregoing development has been reported in the literature. It is referenced here:

"The Excitation of Surface Currents by Electromagnetic and Electrokinetic Waves on a Plasma Immersed Cylinder: I. The Vacuum Sheath," (with A. Olte), Radio Science, 1, No. 8, 977 993, Aug. 1966.

"The Excitation of Surface Currents by Electromagnetic and Electrokinetic Waves on a Plasma Immersed Cylinder: II. The Inhomogeneous Sheath, "(With A. Olte), Radio Science 1, No. 12, 1425-1433, Dec. 1966.

"Surface Current Excitation on an Inhomogeneously-Sheathed Plasma Immersed Cylinder by Electromagnetic and Electrokinetic Waves, Canadian J. Physics, Vol. 45, 1967.

"Admittance Dependence of the Infinite Cylindrical Antenna Upon Exciting Gap Thickness," Radio Science, Vol. 2, No. 12, Dec. 1967.

"Electromagnetic Wave Scattering from a Cylinder Immersed in a Warm Plasma," Radio Science, Vol. 2, No. 12, Dec. 1967.

"Admittance of the Infinite Cylindrical Antenna in a Lossy Incompressible, Magnetoplasma," Canadian J. Physics, Dec. 1967.

"The Admittance of the Infinite Cylindrical Antenna Immersed in a Lossy, Compressible Plasma," Jan. 1968 IEEE-PGAP Trans.

"An Approximate Formula for the Admittance of a Long, Thin Antenna," Jan. 1968 IEEE-PGAP Trans.

"The Excitation of Surface Currents by Electromagnetic and Electrokinetic Waves on a Plasma-Immersed Cylinder," Fall URSI Meeting, Hanover, N. H., (with A. Olte), October 1965.

"The Scattering of Electromagnetic and Electrokinetic Waves Obliquely Incident on an Inhomogeneously-Sheated Plasma Immersed Cylinder," Spring URSI Meeting, Washington, D. C., April 1966.

"Electromagnetic Wave Scattering from a Cylinder in a Warm Plasma," Spring URSI Meeting, Ottawa, Canada, May 1967.

"The Admittance Variation About the Plasma Frequency of an Infinite Dipole Antenna in an Ionospheric Type Plasma," Sprin URSI, Ottawa, Canada, May 1967.

"Antenna Admittance in a Compressible Magnetoplasma," Fall Plasma Physics Meeting, Austin, Texas, Nov. 1967.

"Excitation of Surface Currents on a Plasma-Immersed Cylinder by Electromagnetic and Electrokinetic Waves," Report 05627-4-S, 97 pgs., September 1966.

"Surface Current Excitation on an Inhomogeneously-Sheathed Plasma Immersed Cylinder by Electromagnetic and Electrokinetic Waves, Report 05627-5-S, 30 pgs., December 1966.

"The Scattering of Electromagnetic Waves from a Plasma-Immersed Cylinder," Report 05627-6-S, 21 pgs., December 1966.

"The Admittance of the Infinite Cylindrical Antenna in a Lossy, Isotropic, Compressible Plasma," 82 pgs., Report 05627-10-S, March 1967.

"The Admittance of the Infinite Cylindrical Antenna in a Lossy Plasma II. The Incompressible, Magnetoplasma," Report 05627-11 S, 48 pgs., May 1967.

"Admittance of the Infinite Cylindrical Antenna in a Lossy Plasma III. The Compressible, Magnetoplasma," Report 05627-13-S, 53 pgs., October 1967.

"The Admittance of an Infinite Cylindrical Antenna in Lossy, Compressible, Anistropic Plasma," Canada Journal Physics, 46, 1109, 1968.

The following reports by H. F. Schulte are also related to the election density technique development:

"Antenna Admittance in an Ionospheric-Type Plasma", with E. K. Miller, Plasma Waves in Space and the Laboratory, NATO Advanced Study Institute, NATO Advanced Study Institute, Roros, Norway, April, 1968. (In Press).

"Ionospheric Electron Density Measurements Part I. Results from Three RF Swept Frequency Techniques," URSI Meeting, Washington D. C., April 1968.

"Ionospheric Electron Density Measurements Part II. A Comparison of Experiment and Theory for an Antenna in the Ionosphere", with E. K. Miller and J. W. Kuiper, URSI Meeting, Washington, D. C., April, 1968.

"Antenna Admittance in an Ionospheric Type Plasma," Scientific Report No. 05627-18-S, High Altitude Engineering Laboratory, Dept. of Aerospace Engineering, April, 1968.

The second experimental technique developed for small satellites with partial support from this contract is that of measuring ion energy, and hence temperature, with an hyperbolic retarding potential analyzer (HARP). This device also will be used in a rocket flight. It will be carried on a Nike Tomahawk in the fall of 1968 and the results will be reported under Contract No. NASr-54(05).

For the past several years Prof. W. C. Nelson of the Department of Aerospace Engineering at Michigan has conducted a course called Aerospace System Design for seniors and first year graduate students in which a significant spacecraft or space system is designed on a project basis. These courses have resulted in gratifying stimulation to, and interest on the part of, the students as they participate in a management and technical exercise with many real-life situations. In the fall term of 1967 through a cooperative arrangement

between Prof. Nelson and the investigators of this contract, a small aeronomy satellite, with nearly the same mission as that being worked on for the contract, was assigned as the class project. Many of the actual design constraints which had been developed for the NASA-sponsored satellite were embodied in the student design. Mr. H. F. Schulte in particular, and other investigators of this contract to a lesser degree, worked intimately with the students in explaining and detailing the mission requirements. As a consequence the student satellite STRATUM embodies most of the ideas for a small aeronomy satellite developed under this contract. The invaluable aid of experts from industry who lectured to the design class on specialized topics is hereby acknowledged. The total effort is represented in a report entitled Project Stratum of 6 December 1967. Copies of the Stratum report are being supplied together with this Final Report.

In addition to the aid which industry gave to the student project much help was received on the specific design effort being conducted professionally under the contract. We wish to acknowledge the industrial contributions which were made in the reports on the following pages.

Spacecraft Department, General Electric Co.,

Preliminary Design Considerations for a University of Michigan

"Michael Satellite. August 1965

"1.0 Introduction

"In the following " Preliminary System Design Considerations" for the University of Michigan's MICHAEL satellite, the Spacecraft Department of the General Electric Company has attempted to identify those system design parameters related to the successful accomplishment of the proposed scientific mission.

"The strong relationships between the passive attitude control system and the spacecraft design, discussed in subsequent sections, prompted GE to investigate the feasibility of utilizing an existing vehicle for this application. The "Gravity Gradient Test Satellite" which we have designed and are currently building for the U.S. Air Force is configured with a "double dumbell" gravity gradient system. The AERO-MAGS system, previously proposed, is essentially a swept-back version of the GGTS configuration. It was concluded, that with a minimum design modification, a small satellite compatible with a standard Scout booster could evolve.

"Working from the University of Michigan's design criteria and experimental payload requirements, a preliminary systems analysis was made of the subsystems interacting with the attitude control/vehicle system. The optimized configuration we are proposing should meet the mission requirements and provide sufficient payload capability, sensor location flexibility, adequate power, and design confidence to proceed into an engineering phase.

"More thorough work, however, is required in the area of thermal analysis, and an engineering approach towards the resolution of the outgassing and accomodation coefficient experimental interface should be explored.

"An initial investigation of the outgassing/accomodation coefficient effects indicates a combination coating material/mechanical design approach is feasible. We are prepared to discuss both of these areas at the University of Michigan's convenience."

Convair Division, General Dynamics, OVI

Application to University of Michigan Satellite "Michael" Report

No. GDC DCJ 67-002. Feb. 1967

"FOREWORD

"Convair division of General Dynamics has prepared this preliminary report for the University of Michigan MICHAEL Study Group to serve as an application manual for the integration of MICHAEL experiments into the OV1 satellite.

"This report is preliminary in the sense it provides only the framework of the OV1 application to MICHAEL. It is planned that a follow-up report with specific guidlines, design parameters, performance, cost, etc. will be prepared when the experiment characteristics and interfaces are more clearly defined. It is hoped the enclosed application information will be of benefit to the experiment designer in establishment of his design constraints. In some instances where an example provides a better understanding, OV1 serves to provide quantitative data. OV1-11 is selected because of its similarity to the MICHAEL mission. OV1-11 is to be launched into a 300-n. mi. polar orbit in May 1967. It will carry the latest type Convair gravity gradient system. A list of the OV1-11 experiments and other pertinent data are to be found in Section 7.0.

"Other sections of the report pertain to basic descriptions of the OV1 systems and methods of application. Of particular interest is experiment

integration discussed in Section 6.0 which provides the experimenter with a complete series of events that normally take place from integration sequences, responsibilities, checkouts through to final launch.

"The Convair division looks forward to participation with the University of Michigan in the development of the MICHAEL program."

Space-General Corporation, A Proposal for Basic Structure, Power Supply, and Thermal Analysis for University of Michigan Michael Satellite, SGC-6410, Vol. I, April 1965.

"Introduction

"Space-General Corporation is pleased to submit this proposal to the University of Michigan to provide satellite structures, power supplies, and thermal analysis for the MICHAEL Aeronomy Satellite. This proposed program matches well with the existing Space-General satellite system development programs and with the overall space systems aims of the corporation.

"The general utility satellite as designed for the Air Force under Contract AF 19(628)-4775 offers many advantages for use in the MICHAEL Satellite application. The general arrangement offers substantial flexibility in the locations of sensors and supporting electronic systems. The entire shelf assembly is available for equipment installations with sufficient space to allow judicious placement of the components to achieve the desired balance and moments of inertia. Generally speaking, sufficient space on the platform is available to allow installations without the complications of additional bracketry.

The modular and interchangeable arrangement of the solar arrays offers the advantages of easy access to all portions of the satellite through removal of any one or all of these panels. Since each of these panels is relatively small, the cost of spares, assuming one spare for each panel type, can be kept to a minimum.

"Several additional advantages would accrue as a result of using the general utility satellite design. Some experiments which will be carried on the Air Force OV3 satellite series will be very sensitive to out-gassing. Quantitative measurements will be made, within the limits of vacuum testing facilities, to determine levels of out gassing of all non metallics. This data will be available for use in selection of materials perculiar to the MICHAEL satellite.

"The testing program for the OV3 spacecraft will include vibration and shake tests using a structural dynamic model which is substantially equivalent to that being proposed under Option 1 of this proposal. These tests will include the use of the SLV-1A (SCOUT) "E" Section. Data from these tests will establish definite local environments for some special payload configurations. This data would be of great value for use in design of other payloads assuming some degree of similarity. Additionally, the obvious feature of having a structure for the MICHAEL Satellite which has been previously qualified to withstand the rather severe environment imposed by the LSV-1A would be of great advantage.

"Our personnel are well acquainted with structural design, power supply design, and thermal analysis of satellites. SGC is presently involved in the design of aforementioned four complete satellite systems for the Air Force, and has extensive experience in sounding rockets, sounding rocket payloads, upper stage launch vehicle systems, guidance and control systems, and unmanned lunar reconnaissance probes. SGC has also provided data systems for Ranger 1 and 2 and has flown one of the first successful data coding devices,

the Digilock system. Further personnel who will be associated with the proposed program have participated in and contributed to other space programs such as Rangers 3, 4, 5, 6, 7, Mariner A and Mariner 2 as well as the current Mariner 4. In summary, this proposal makes available a highly capable and experienced team, for the accomplishment of the program for the MICHAEL Satellite."

The studies undertaken for this contract have advanced the understanding of the application and performance of mass spectrometers in making composition and temperature measurements in an aeronomy satellite and will be useful in preparing a proposal at the appropriate time for one version of such a satellite.

The Measurement of Neutral Gas Temperature

P. B. Hays
K. D. McWatters

Abstract

A method to directly measure the neutral gas temperature at satellite altitudes is presented. A mass spectrometer is used in each of two cavities so that the number densities of two gases can be examined. The angular orientation of the cavities and the mass spectrometers are two major sources of error. A single gas analysis does not eliminate the angular orientation error. A two gas analysis using helium and nitrogen appears feasible for measuring the ambient temperature. The heavy gas is used to determine the orientation of the cavities with respect to the velocity vectors of the satellite. Since errors in temperature are related to instrument error only, a more refined measurement can be achieved. Two basic configurations are considered.

Introduction

The ambient kinetic temperature is required in order to study the energy balance and heating in the thermosphere. The temperature of the atmosphere at altitudes in excess of 200 km is deduced at present from the total gas density data obtained from orbital decay studies (Jacchia, 1963) and from density scale heights determined from density-altitude profiles (Newton, Howowitz, and Priester, 1965). The orbital decay technique has been to match the experimental density with the density obtained from a model and accept the model temperature as the actual atmospheric temperature. This process yields at best an average temperature and may be grossly in error. Stein and Walker (1965) have investigated the effect on the derived temperature of using constant composition at the base level, i.e. 120 km, and have found that errors of the order of 25% are not unlikely. The density scale height technique has been to use the density data derived from a total pressure gauge measurement and mean mass values as simultaneously determined by a mass spectrometer. The temperature uncertainty using this method is thought to be $\pm$ 20%. Temperatures errors of 20% or greater would certainly be intolerable if these temperature measurements are to be used to study the energy balance and heating in the atmosphere.

It has been suggested that a direct measurement of temperature could be made using two density gauges oriented at 90° from each other (Isakov, 1963). This technique does not appear feasible when the accuracy requirements are analyzed realistically. A more realistic approach has been suggested where a mass spectrometer is used in each of two cavities so that a single gas such as helium can be examined (Chizhov, 1963). The errors are reduced by using

a single gas with low molecular weight, however, the major source of error, that associated with measuring the angular orientation of the cavities, still remains.

A method for reducing the sensitivity to angular errors has been investigated. The necessity to measure orientation directly was supplemented by the measurement of two separate gases in each of the two cavities. The light gas gives information about temperature and the heavy gas is used to determine the orientation of the instrumentation with respect to the velocity vectors of the satellite.

The following discussion is a brief review of the properties of various cavity arrangements which illustrates the logical progression to the two gas temperature measurement study.

Simple Cavity Theory

One obvious property of the ambient gas which is related to temperature is the molecular flux normal to a unit area.

$$\vec{F}_i = n_i \sqrt{\frac{R_o T_i}{2\pi M_i}}\, \psi(S \cos\Theta)\, \vec{i}_n \tag{1}$$

where

$$\psi(X) = \exp(-X^2) + X\sqrt{\pi}\,(1 + \mathrm{erf}(X)) \tag{2}$$

$$\cos\Theta = \vec{V}\cdot\vec{i}_n/|V|$$

and

$$S_i = V/\sqrt{2R_o T_i/M_i}$$

where n_i is the number density of the i^{th} species in the ambient, T_i is the temperature, M_i is the molecular mass, R_o is the universal gas constant, Si the speed ratio of the i^{th} species molecules through a unit area in the direction of the unit vector $\vec{i}_n$. It is possible to measure the flux F_i by replacing the element of area by a tube leading to a gauge volume, v_c and measuring the properties of the disturbed gas in the cavity. (Harris and Patterson, 1958; Patterson, 1959). The continuity relation states that for the geometry described in Figure 1, the number density of the i^{th} species in the cavity obeys the relation

$$\begin{aligned} v_c \frac{dN_{c_i}}{dt} &= F_{in} - F_{out} \\ &= n_i \sqrt{\frac{R_o T_i}{2\pi M_i}}\, \frac{\pi D_e^2}{4}\, \psi(S_i \cos\Theta)\, W(S, D_e/\ell, \Theta) \\ &\quad - N_{c_i} \sqrt{\frac{R_o T_c}{2\pi M_i}}\, \frac{\pi D_e^2}{4}\, W(0, D_e/\ell, 0) \\ &\quad + \left(\frac{dN_{c_i}}{dt}\right)_{\text{sorption}} \end{aligned} \tag{3}$$

where N_{c_i} is the number density of the i^{th} species in the cavity, T_c is the temperature of the cavity walls, v_c is the volume of the cavity and $W(S, D_e/\ell, \Theta)$ is a factor used to account for the reduction of flow through a tube of length ℓ and diameter D_e compared to an orifice of the same diameter. (Clausing, 1932; Repnev, 1960).

The term $\left.\frac{dN_{c_i}}{dt}\right|_{\text{sorption}}$ refers to the effect of sorption processes on the number of particles in the cavity. Gases may either be physically or chemically absorbed on a surface. If chemically inert surfaces such as gold are utilized inside the cavities one would expect a decrease in the amount of chemical adsorbtion (deBoer, 1953; Smithells, 1937). Molecules with adsorption energies less that 15 kilocalories per mole will not adsorb on a surface at pressures of 10^{-4} torr at room temperature (Bromwell, 1965). Therefore, there will be little, if any, adsorption of gases such as helium, nitrogen and argon and an adsorption equilibrium for these gases will be quickly established. That is, the number of molecules being adsorbed will equal those being desorbed and $\left.\frac{dN_{c_i}}{dt}\right|_{\text{sorption}}$ may be considered negligible for the above mentioned gases. Information is not available on the heats of adsorption of atomic and molecular oxygen on gold. If the heats of adsorption for these two gases are within the physical adsorption realm, one would again expect little adsorption and an adsorption equilibrium would be quickly established. If atomic or molecular oxygen chemically adsorb, the time to reach equilibrium would certainly be longer. Also if there is appreciable adsorption of atomic oxygen, the surface would act as a catalyst for the recombination of atomic oxygen which must be considered in calculating the required time before an adsorption equilibrium for this gas is established. However, since the gases under consideration for the two cavity method for deriving temperature are helium, nitrogen and argon and the time required for these gases to reach an adsorption equilibrium is small, one may proceed assuming $\left.\frac{dN_{c_i}}{dt}\right|_{\text{sorption}}$ negligible.

Now returning to the discussion of the conditions inside a cavity, assuming the sorption term is negligible, one finds that if the exterior flow is steady (i.e. S_i = const), the cavity equation can be integrated to give

$$\frac{N_{c_i}}{n_i} = \frac{N_{c_i}(0)}{n_i} e^{-t/\tau} + \sqrt{\frac{T_i}{T_c}}\,\psi(S_i\cos\Theta)\,\frac{W(S_i, D_e/\ell, \Theta)}{W(0, D_e/\ell, 0)}\left[1-e^{-t/\tau_c}\right] \qquad (5)$$

where

$$\tau_c = \sqrt{\frac{2\pi M_i}{R_o T_c}}\left(\frac{\nu_c}{\frac{\pi D_e^2}{4}}\right)\frac{1}{W(0, D_e/\ell, 0)} = \text{cavity time constant}$$

For a cylindrical cavity of length L and cross-sectional area A the time constant τ_c becomes

$$\tau_c = \sqrt{\frac{2\pi M_i}{R_o T_c}}\, L\left(\frac{A}{\frac{\pi D_e^2}{4}}\right)\frac{1}{W(0, D_e/\ell, 0)}$$

As an example, assume a large cavity, L = 1 meter, $\frac{A}{\frac{\pi D_e^2}{4}} = 50$, T=50°C,

$W(0, D_e/\ell, 0) = 1$ and $M_i = 4$, we find that

$$\tau_c = .153 \text{ sec}$$

Thus, for the situation where the time rate of change of the sorption processes may be neglected, the time constant for a large cavity is sufficiently small to be negligible. In this situation

$$\frac{N_{c_i}}{n_i} = \sqrt{\frac{T_i}{T_c}}\,\psi(S_i\cos\Theta)\,\frac{W(S, D_e/\ell, \Theta)}{W(0, D_e/\ell, 0)} \qquad (6)$$

From these relations expressing the density in the cavity as a function of the ambient number density and temperature, one observes that two measurements of cavity density at varying values of Θ are sufficient to determine ambient number density and temperature.

The theory presented above can now be applied to the development of various temperature sensors. Theoretically, if the number density of a given species of neutral gas is measured in two cavities operating at different values of Θ and the gas is assumed to be thermally accomodated to the cavity wall temperature, the ambient number density and temperature of the gas species can be determined. However, in practice, errors in the number density measuring device (i.e. mass spectrometer) and in the angle Θ are of prime importance. It is necessary to determine a configuration of the two required cavities such that these errors have the minimum effect on the calculated temperature. In the present investigation two basic geometrical configurations have been studied.

Configuration 1

The first geometrical configuration considered was that of two identical cavities for which the inlet orifices are separated by the angle $\Delta\Theta$, and which have the mean angular position Θ with respect to the free stream vector, as pictured in Figure 2.

The general steady state cavity relation (6) presented above may be used to determine the ratio or the number densities measured in the two cavities with $W(S,\infty,\Theta) = 1$.

$$R = \frac{N_1}{N_2} = \frac{\exp(-S_1^2) + \sqrt{\pi}\, S_1(1+\mathrm{erf}S_1)}{\exp(-S_2^2) + \sqrt{\pi}\, S_2(1+\mathrm{erf}S_2)} = \frac{\psi(S_1)}{\psi(S_2)} \qquad (7)$$

where N_1 and N_2 are the number densities of the same species in cavity one and two respectively and

$$S_1 = V\cos(\Theta - \Delta\Theta/2)\Big/\sqrt{\frac{2R_o T_i}{M_i}} = S_o\cos\left(\Theta - \frac{\Delta\Theta}{2}\right)$$

$$S_2 = V\cos(\Theta + \Delta\Theta/2)\Big/\sqrt{\frac{2R_o T_i}{M_i}} = S_o\cos\left(\Theta + \frac{\Delta\Theta}{2}\right)$$

Notice that the ratio, R, depends entirely upon the free stream temperature and the orientation angle Θ when V and $\Delta\Theta$ are fixed. Once R and Θ are known the temperature is determined.

Single Gas Error Analysis for Configuration 1

Since R and Θ are subject to measuring errors, one must determine the sensitivity of the temperature to errors in these two quantities. The error analysis for configuration 1 follows.

A small change δT (T is assumed equal to T_i) and $\delta\Theta$ in relation (7) results in the change

$$\delta R = \frac{\partial R}{\partial T}\delta T + \frac{\partial R}{\partial \Theta}\delta\Theta \tag{8}$$

or the temperature error is

$$\delta T = \frac{\delta R - \frac{\partial R}{\partial \Theta}\delta\Theta}{\frac{\partial R}{\partial T}}$$

Here

$$\frac{\partial R}{\partial T} = \frac{\sqrt{\pi}}{2}\frac{R}{T}\left\{\frac{(1+\mathrm{erf}S_2)S_2}{\psi(S_2)} - \frac{(1+\mathrm{erf}S_1)S_1}{\psi(S_1)}\right\}$$

and

$$\frac{\partial R}{\partial \Theta} = \sqrt{\pi}\, S_o R\left\{\frac{(1+\mathrm{erf}S_2)\sin(\Theta+\frac{\Delta\Theta}{2})}{\psi(S_2)} - \frac{(1+\mathrm{erf}S_1)\sin(\Theta-\frac{\Delta\Theta}{2})}{\psi(S_1)}\right\}$$

However since errors δR and $\delta\Theta$ are assumed to be random, the rms error in temperature becomes

$$\sqrt{\overline{\delta T^2}} = \sqrt{\frac{\overline{\delta R^2}}{(\partial R/\partial T)^2} + \left(\frac{\partial R}{\partial \Theta}\Big/\frac{\partial R}{\partial T}\right)^2\overline{\delta\Theta^2}} \tag{9}$$

where $\sqrt{\overline{R^2}}$ and $\sqrt{\overline{\delta\Theta^2}}$ and the rms errors in measured values of R and Θ

respectively. The error in R is related to the individual measurements of number density made in the two cavities. Let

$$\begin{aligned} N_1' &= N_1 + \epsilon_1 N_1 \\ N_2' &= N_2 + \epsilon_2 N_2 \end{aligned} \tag{10}$$

where $\epsilon = \frac{\delta N}{N}$ and the prime denotes the measured quantity which is in error. Combining these relations one finds that

$$R + \delta R = \frac{N_1+\epsilon_1 N_1}{N_2+\epsilon_2 N_2} = \frac{N_1+\delta N_1}{N_2+\delta N_2}$$

$$R + \delta R \approx \frac{N_1}{N_2}\left(1+ \frac{\delta N_1}{N_1} - \frac{\delta N_2}{N_2} + \ldots\right) \tag{11}$$

Thus for a random ϵ one finds that the rms error in R is

$$\sqrt{\overline{\delta R^2}} = R\left[\frac{\overline{\delta N_1^2}}{N_1^2} + \frac{\overline{\delta N_2^2}}{N_2^2}\right]^{\frac{1}{2}} \tag{12}$$

Thus the rms error in the temperature in terms of the orientation error and the instrumentation error is

$$\sqrt{\overline{T^2}} = \left\{ \frac{R^2\left[\frac{\overline{\delta N_1^2}}{N_1^2} + \frac{\overline{\delta N_2^2}}{N_2^2}\right]}{\left(\frac{\partial R}{\partial T}\right)^2} + \left(\frac{\partial R}{\partial \Theta}\Big/\frac{\partial R}{\partial T}\right)^2 \overline{\delta\Theta^2} \right\}^{\frac{1}{2}} \tag{13}$$

One may consider the instrumentation error composed of two sources; that due to calibration and that due to sensitivity. The instrumentation error is proportional to the calibration error and inversely proportional to the sensitivity of the instrument. Since the calibration error represents a bias in measuring the correct number density and sensitivity represents a random error, these two errors are combined in a rms fashion to represent the total number density

error for a given species. Thus, the rms number density error may be expressed as

$$\sqrt{\frac{\overline{\delta N^2}}{N^2}} = \left(\eta^2 + \frac{\overline{X^2}}{N^2} \right)^{\frac{1}{2}}$$

where η is the percent calibration error and X is the instrument sensitivity. Thus, a 100% error in the number density is assumed due to instrument sensitivity when the quantity being measured is equal to the sensitivity of the instrument. The instrument sensitivity is assumed to be $1.5*10^5$ particles/cm^3. This sensitivity represents the sensitivity when the peak deflection is 2 times the peak noise; i.e. at 100% signal to noise ratio.

Relation (13) for the rms temperature error now becomes

$$\sqrt{\overline{\delta T^2}} = \left\{ \frac{R^2[2\,\overline{\eta^2}]}{\left(\frac{\partial R}{\partial T}\right)^2} + \frac{R^2\left[\frac{\overline{X^2}}{N_1^2} + \frac{\overline{X^2}}{N_2^2}\right]}{\left(\frac{\partial R}{\partial T}\right)^2} + \left(\frac{\partial R}{\partial \Theta} \Big/ \frac{\partial R}{\partial T}\right)^2 \overline{\delta\Theta^2} \right\}^{\frac{1}{2}} \qquad (14)$$

This relation is illustrated in Figure 3 for helium with $\Delta\Theta=90^o$. The three sources of error are plotted individually assuming a calibration error of 1 per cent and an instrument sensitivity as mentioned above. The number density ratio of that in the aft cavity to that in the ambient is also plotted. The ambient density was that of the 1965 CIRA Atmosphere at 300 km for mean solar activity at the 10th hour. The ambient temperature was assumed to be 1500^oK. The temperature of the cavity walls was assumed to be 323^oK. The velocity of the satellite was assumed to be 7.5km/sec. The ambient helium number density was assumed to be $4.56*10^6$ particles per cm^3. Notice that as Θ increases beyond 50^o the error due to instrument sensitivity increases due to the small value of number density in the aft cavity while the

error due to the orientation error is approaching a minimum. Conversely, when the error due to instrumentation errors is small, the error due to the orientation error is prohibitive. Thus, it appears that with this geometry, using a single gas, the errors are too large to allow a meaningful measurement of temperature.

However it appears that the ideal situation would be if a maxima in R occurred where Θ had a value such that the aft cavity contained a measurable amount of gas. Secondly, the orientation error appears to be the most severe source of error, thus particular attention should be applied to minimizing this effect.

Configuration 2

Examination of the previous hypothetical temperature probe led to consideration of the geometry shown in Figure 4. For this configuration with $W(S, D_e/\ell, \Theta) = 1$

$$R = \frac{\exp(-S_1^2)+\sqrt{\pi}\, S_1(1+\mathrm{erf}S_1)}{\exp(-S_2^2)+\sqrt{\pi}\, S_2\mathrm{erf}S_2} = \frac{\psi(S_1)}{\psi(S_2)-\sqrt{\pi}\, S_2} \qquad (15)$$

where

$$S_1 = S_o\cos\Theta$$

$$S_2 = S_o\sin\Theta$$

The ratio for helium is presented in Figure 5. Notice in Figure 5 that R has a maxima at $\Theta=0^o$ where it can be shown that $N_{2_i}/n_i > 1$. This indicates that this geometry should be superior in terms of sensitivity to angular and instrumentation errors

In this case the relation (14) for the rms temperature error is still valid

$$\sqrt{\overline{\delta T^2}} = \left\{ \frac{R^2\left[\overline{p_n^2}\right]}{\left(\frac{\partial R}{\partial T}\right)^2} + \frac{R^2\left[\frac{\overline{X^2}}{N_1^2} + \frac{\overline{X^2}}{N_2^2}\right]}{\left(\frac{\partial R}{\partial T}\right)^2} + \left(\frac{\partial R}{\partial \Theta} \Big/ \frac{\partial R}{\partial T}\right)^2 \overline{\delta\Theta^2} \right\}^{1/2} \qquad (14)$$

where in this case

$$\frac{\partial R}{\partial T} = \frac{\sqrt{\pi}}{2T}\left\{\frac{S_2 R\ \mathrm{erf}\ S_2 - (1+\mathrm{erf}\ S_1)\ S_1}{\psi(S_2) - \sqrt{\pi}\, S_2}\right\} \qquad (16)$$

$$\frac{\partial R}{\partial \Theta} = -\sqrt{\pi}\left\{\frac{S_2(1+\mathrm{erf}\ S_1)+S_1 R\,\mathrm{erf}\ S_2}{\psi(S_2) - \sqrt{\pi}\, S_2}\right\}$$

The three sources of error are plotted individually in Figure 6 assuming a calibration error of 1 percent and an instrument sensitivity of $1.5*10^5$ particles per cm^3. The number density ratio of that in the aft cavity to that in the ambient is also plotted. The ambient conditions are the same as used in presenting the errors for configuration 1. The large error due to the instrument sensitivity associated with configuration 1 is not a condition of configuration 2. It is interesting to note that the major difficulty with this configuration is again the sensitivity of the temperature error to the orientation error. As Θ increases beyond 3^o, the temperature error due to the orientation error becomes predominant. The difficulty of maintaining a 3^o orientation with respect to the free stream vector at all times eliminates this configuration, using a single gas, as a temperature measuring device.

One further difficulty with configuration 2 is the effect of the tubular construction of the aft cavity on the flow in the cavity. In the above analysis $W(S, \infty, \Theta)$ was assumed equal to 1 and $W(0, De/\ell, 0)$ was assumed equal for both cavities. These assumptions are not quite proper. The transmission probability for the aft cavity of configuration 2 is less that 1(Ballance, 1966). That is, of the total number of particles entering a tubular cavity, only a certain percentage will reach the ionizing region due to surface effects. This makes the

data analysis of this configuration more difficult as the transmission probability is a function of the size and shape of the cavity, the flow speed, the flow direction relative to the orifice, and the molecular weights of the molecules involved.

Two - Gas Temperature Measurements

The error due to the orientation error for both configurations considered was prohibitive. A method to eliminate the orientation error was sought and it was felt that the measurement of a heavier gas might define the orientation of the satellite. Configuration 1 was analyzed with both helium and nitrogen and $\Delta\Theta = 90^{o}$. In Figures 7 and 8 plots of R vs. Θ are presented for helium and nitrogen respectively. Cross plotting of Figures 7 and 8 leads to contours of constant R for both helium and nitrogen which are presented in Figure 9. It is obvious that nitrogen could not be used to determine temperature since a small variation in Θ would correspond to an extremely large change in temperature. However, the heavy gas could serve as an angular measure. That is, if both the ratio for nitrogen and helium are measured, the temperature can be determined without knowledge of the angle Θ. If this situation is exploited the only errors would be those in the measurement of the ratios for nitrogen and helium.

The error in the temperature resulting from errors in the measured ratios of helium and nitrogen would then be

$$\sqrt{\overline{\delta T^2}} = \left\{ \left(\frac{\partial T}{\partial R_H}\right)^2_{R_N} \overline{\delta R_H^2} + \left(\frac{\partial T}{\partial R_N}\right)^2_{R_H} \overline{\delta R_N^2} \right\}^{\frac{1}{2}} \qquad *(17)$$

* $\left.\frac{\partial y}{\partial x}\right|_z$ is the partial derivative of y with respect to x when z is left constant

where

$$\left.\frac{\partial T}{\partial R_H}\right|_{R_N} = \left(\left.\frac{\partial R_H}{\partial T}\right|_{\Theta} - \left.\frac{\partial R_N}{\partial T}\right|_{\Theta} \left.\frac{\partial R_H}{\partial \Theta}\right|_{T} \Big/ \left.\frac{\partial R_N}{\partial \Theta}\right|_{T} \right)^{-1} \tag{18}$$

and

$$\left.\frac{\partial T}{\partial R_N}\right|_{R_H} = \left(\left.\frac{\partial R_N}{\partial T}\right|_{\Theta} - \left.\frac{\partial R_H}{\partial T}\right|_{\Theta} \left.\frac{\partial R_N}{\partial \Theta}\right|_{T} \Big/ \left.\frac{\partial R_H}{\partial \Theta}\right|_{T} \right)^{-1} \tag{19}$$

Here again the errors in the ratios are functions of the individual instrument errors, thus, one can write as follows

$$\sqrt{\overline{\delta T^2}} = \left\{ \begin{array}{l} \left(R_H \frac{\partial T}{\partial R_H \partial R_H}\right)^2 \left[2\eta^2\right] + \left(R_H \frac{\partial T}{\partial R_H}\right)^2 \left[\frac{\overline{X^2}}{N^2_{H_1}} + \frac{\overline{X^2}}{N^2_{H_2}}\right] \\ + \left(R_N \frac{\partial T}{\partial R_N \partial R_N}\right)^2 \left[2\eta^2\right] + \left(R_N \frac{\partial T}{\partial R_N \partial R_N}\right)^2 \left[\frac{\overline{X^2}}{N^2_{N_1}} + \frac{\overline{X^2}}{N^2_{N_2}}\right] \end{array} \right\}^{\frac{1}{2}} \tag{20}$$

This equation has been evaluated for a calibration error of 1 per cent and an instrument sensitivity of $1.5*10^5$ particles per cm^3. The ambient conditions are the same as used in presenting the errors for a single gas analysis of configurations 1 and 2. The ambient nitrogen number density assumed was $2.12*10^8$ particles per cm^3. Three sources of error, the calibration errors for helium and nitrogen and the sensitivity error for helium,are presented in Figure 10. The fourth error, the sensitivity error for nitrogen, is quite small (1 ^oK) at an altitude of 300 km and is indicative of the comparitively large number density of nitrogen in the aft cavity. The decrease of the helium

number density in the aft cavity as Θ increases has caused the temperature error due to instrument sensitivity to increase. The decrease of the temperature error due to the calibration error as Θ increases is due to the fact that $-\frac{\partial T}{\partial R}$ decreases more rapidly than R increases.

A similar two gas analysis has been made for configuration 2. The helium and nitrogen ratios are shown in Figures 5 and 11 respectively. The contour plot for this configuration is shown in Figure 12. The three main sources of error are presented in Figure 13. The fourth error, the sensitivity error for nitrogen, is also small ($< 1^{o}K$) for this configuration at an altitude of 300 km.

The use of nitgrogen as the heavy gas for determining the orientation of the satellite is questionable. Mass spectrometer measurements in a cavity are troubled with the formation of CO by the interaction of O and O_2 with carbon containing metals. Neir et al. (1964) have found in laboratory tests that the carbon monoxide residual will rise with the introduction of O_2 into the system. The contribution to the 28 peak by CO may be a serious source of error in measuring the correct nitrogen number density. The use of argon as the heavy gas, although less dense than nitrogen in the atmosphere, was investigated. Relation (20) has been evaluated for a calibration error of 1 percent and an instrument sensitivity of $1.5*10^{5}$ particles per cm^3 for configuration 1. The ambient conditions are the same as used in presenting the previous errors. The ambient argon number density assumed was $1.66*10^{5}$ particles per cm^3. The four sources of error are presented in Figure 14. The sensitivity error for argon is the most prohibitive error. It is obvious a more sensitive instrument is required if argon is to be used as the heavy gas for the angular measurement.

So far, the temperature errors for both configurations have been presented in terms of 1 percent calibration error and an instrument sensitivity of $1.5*10^5$ particles per cm^3. It would be of interest to determine the total rms temperature error assuming a reasonable calibration error and using the same instrument sensitivity. It is important to note that the two instruments could have large calibration errors but if the errors were of equal magnitude and of the same sign, the correct ratio, R, could still be determined. This can be seen by looking at relation (11). It is therefore necessary to estimate the relative calibration error of the two instruments. For the purpose of this analysis, the relative calibration error was assumed to be 5 percent. Relation (20) has been evaluated for both configurations with a 2.5 per cent calibration error assigned to each instrument and an instrument sensitivity of $1.5*10^5$ particles per cm^3. The total rms temperature errors for configuration 1 at altitudes of 300, 400 and 500 km are presented in Figure 15, using helium and nitrogen as the two gases. The ambient conditions are the same as used previously. The ambient helium number densities assumed at 400 and 500 km were $3.22*10^6$ and $2.35*10^6$ particles per cm^3 respectively. The ambient nitrogen number densities assumed at 400 and 500 km were $2.10*10^7$ and $2.36*10^6$ particles per cm^3 respectively. The minimum percentage temperature errors for configuration 1 at altitudes of 300, 400 and 500 km are ± 12.5, ± 13.8, and ± 15.9 percent respectively. It must be remembered that these are the minimum errors as the satellite, although passively stabilized, will oscillate and will come into the favorable angular conditions only periodically. At large values of Θ the number density in the aft cavity might be influenced by the free outgassing of its surfaces. The nitrogen number density in the aft cavity due to the flow of the ambient gas into the cavity is equal to that in the ambient at a value of $\Theta = 48^o$. The corresponding angular value for helium

is $\Theta = 52^{\circ}$ (Figure 3). The contribution to the 28 and 4 peaks from free outgassing of the cavity surfaces becomes more significant as Θ increases. This is discussed more thoroughly in the section under Surface Outgassing. This effect has not been included in this error analysis. Suffice it to say, the free outgassing rates of the aft cavity surfaces should be experimentally determined to see what effect these rates have on the temperature error at large values of Θ for configuration 1.

The total rms temperature errors for a 2.5 percent calibration error and a sensitivity of $1.5*10^5$ particles per cm^3 at altitudes of 300, 400 and 500 km are presented in Figure 16 for configuration 2, using helium and nitrogen as the two gases. The ambient conditions are the same as used previously. The minimum percentage temperature errors for configuration 2 at altitudes of 300, 400 and 500 km are ± 9.1, ± 9.8 and ± 11 percent respectively. These errors are less than those for configuration 1 but one must remember the inherent difficulty in analyzing this configuration due to its tubular construction. The ratio of the number density in the aft cavity to that in the ambient is always equal to or greater than 2.15 (Figure 6), assuming a transmission probability of one. Therefore, the temperature error due to free outgassing of the cavity surfaces will not be as severe in this configuration as it is at large values of Θ in configuration 1.

Configuration 1 has also been analyzed for $\Delta\Theta = 60^{\circ}$ and 30°. The total rms temperature errors for a 2.5 percent calibration error and a sensitivity of $1.5*10^5$ particles per cm^3 at altitudes of 300, 400, and 500 km are presented in Figure 17 for configuration 1, using helium and nitrogen as the two gases, with $\Delta\Theta = 30^{\circ}$. The minimum percentage temperature errors for this arrangement at altitudes of 300, 400, and 500 km are ± 10.1, ± 11.7 and ± 14.0 percent respectively.

Therefore, an angular separation of 30°, instead of 90°, for the two cavities of configuration 1 represents a slight improvement in the total rms temperature error. The problem of free outgassing of the cavity surfaces is also present in this arrangement of configuration 1. The free outgassing rates of the aft cavity surfaces should be considered, at large values of Θ , to see what effect these rates have on the temperature error.

Instrument Drift

One of the most serious sources of error that has not been included is the systematic drift of one or both of the mass spectrometers used to measure the number densities in the cavities. This effect is illustrated in Figure 18 which has instrument calibration drift lines superimposed on the contour plot for configuration 2. Notice that a calibration offset corresponds to a nearly constant temperature error, but variations in temperature are retained. This effect is also a condition of configuration 1. Thus, calibration drift errors are not as serious as one would at first expect.

It should be possible, at least in principle, to cross calibrate by mechanically switching the instruments, or to design a mechanical valving system which can effectively transpose the instruments. A satisfactory valve can be obtained if the area of the leakage path is small by comparison with the area of the cavity orifices. This criterion can be met without the use of either an elastic seal or excessively close tolerances. The valve can be made fail safe by designing so that the only mechanically stable positions are those which are fully "open" to either cavity.

It is possible to obtain the correct ratio, R, within the limits of the instrument calibration and sensitivity, even if one or both instruments have drifted if an effective valving system is employed. The information available is as follows

$$R_1 = \frac{N_1(1+\epsilon_1)}{N_2(1+\epsilon_2)} \qquad (21)$$

where R_1 is the number density ratio with the valve in one position, N_1 is the number density of a particular species in cavity 1, N_2 is the number density of the same species in cavity 2, ϵ_1 is the percent drift of instrument 1 and

ϵ_2 is the percent drift of instrument 2. Upon moving the valve into the other position, the two inctruments are now interchanged; i.e. instrument 1 is now measuring the number density in cavity 2 and instrument 2 is now measuring the number density in cavity 1. A different number density ratio is obtained because of the different values for ϵ_1 and ϵ_2. Therefore, a new ratio is available and is expressed as

$$R_2 = \frac{N_1(1+\epsilon_2)}{N_2(1+\epsilon_1)} \tag{22}$$

Dividing R_1 by R_2 yields

$$\frac{R_1}{R_2} = \left(\frac{1+\epsilon_1}{1+\epsilon_2}\right)^2$$

But

$$\frac{N_1}{N_2} = \frac{R_1(1+\epsilon_2)}{(1+\epsilon_1)} = \frac{R_1}{\left(\frac{R_1}{R_2}\right)^{1/2}}$$

Therefore

$$\frac{N_1}{N_2} = \sqrt{(R_1 R_2)} \tag{23}$$

Therefore it is possible, at least in principle, to obtain the correct number density ratio even though the two instruments have drifted. It is not possible to determine the drift of the individual instruments so the absolute value of the number densities cannot be corrected. However, the ambient temperature measurement is dependent on ratios. Since the correct ratios can be determined, even if the instruments drift, the correct ambient temperature can be derived, within the limits of instrument calibration and sensitivity.

Surface Outgassing

The free outgassing rate of the cavity surfaces must be investigated to assure meaningful cavity mass spectrometer measurements at satellite altitudes. Free outgassing is defined as the desorption of gases from and through the surface. Under purely thermal conditions, the monatomic inert gases, argon, helium, etc., do not dissolve in, or permeate, true metals (Dushman, 1962). Nitrogen has been shown to be insoluble, within limits of the experimental method, in cobalt, copper, silver, and gold (Dushman, 1962). However, gases may be trapped in metals during the manufacturing process and are free to desorb at a later time. The problem is then one of diffusion of these trapped gases and desorption of the adsorbed gas phase molecules. Adsorption (the process of a gas dissolving into the interior of a solid) of helium, argon and nitrogen may be neglected if a gold surface is employed.

One may consider the following problem to arrive at the maximum free outgassing rates allowable. Assume a cavity has an area of 300 sq. cm. and a circular orifice with a diameter of 1 cm. One finds, assuming no flow into the cavity and neglecting adsorption of the gas phase molecules by the surface, that the total free outgassing rate sufficient to keep the cavity at a constant number density is

$$\sum_{i=1}^{i=\ell} A_c \, \delta\tilde{t}_i = \sum_{i=1}^{i=\ell} \frac{N_{c_i} \, \bar{C}_i \, A_e}{4} \qquad (24)$$

where $\delta\tilde{t}_i$ is the free outgassing rate of the i^{th} species, $\bar{C}_i$ is the mean speed of the i^{th} species, N_{c_i} is the number density of the i^{th} species, A_c is the area of the cavity surfaces.

The mean speed of the molecules is given by

$$\bar{C} = \sqrt{\frac{8R_o T_i}{\pi M_i}}$$

where R_o, T_i, and M_i are defined as previously.

For the problem under consideration

$$300 \sum_{i=1}^{i=\ell} \delta\tilde{t}_i = \sum_{i=1}^{i=\ell} \frac{N_{c_i} \bar{C}_i A_e}{4} = 2857 \sum_{i=1}^{i=\ell} N_{c_i} \sqrt{\frac{T_i}{M_i}}$$

or the total free outgassing rate, in $\frac{\text{torr-liters}}{\text{sec-cm}^2}$, to keep the gas in the cavity at a constant number density is

$$\sum_{i=1}^{i=\ell} \delta\tilde{t}_i = 2.94*10^{-19} \sum_{i=1}^{i=\ell} N_{c_i} \sqrt{\frac{T_i}{M_i}} \quad \frac{\text{Torr-liters}}{\text{sec-cm}^2}$$

Assuming the gas is in temperature equilibrium with the cavity surfaces (300°K), the free outgassing rates of the three gases under consideration for the ambient temperature experiment are:

$$\delta\tilde{t}_{He} = 2.546*10^{-18} N_{c_{He}}$$

$$\delta\tilde{t}_{N_2} = 9.623*10^{-19} N_{c_{N_2}}$$

$$\delta\tilde{t}_{AR} = 8.051*10^{-19} N_{Ar}$$

One would like to compare the cavity number density due to free outgassing to the number density in the cavity due to the flow of the ambient gas into the cavity. The ambient number densities are given by the CIRA 1965 Atmosphere for mean solar activity and the 10th hour are:

Alt.	He	N_2	Ar
km.	$/cm^3$	$/cm^3$	$/cm^3$
200	$7.49*10^6$	$3.52*10^9$	$8.31*10^6$
300	$4.56*10^6$	$2.12*10^8$	$1.66*10^5$
400	$3.22*10^6$	$2.10*10^7$	$6.24*10^3$
500	$2.35*10^6$	$2.36*10^6$	

The ratio of the number density in the aft cavity to that in the ambient for configuration 1 is greater than 1 for optimum operating angular conditions (Figures 15 and 3). Therefore, assuming the number density in the aft cavity is at least equal to that in the ambient, and if the number density in the cavity due to free outgassing is to be 1% of that in the cavity due to the flow of the ambient gas into the cavity the outgassing rate for helium would be;

$$\delta\tilde{t}_{He} = 2.546*10^{-18}*.01*N_{c_{He}}$$

The allowable free outgassing rates for the three species at the various altitudes are;

Alt.	$\delta\tilde{t}_{He}$	$\delta\tilde{t}_{N_2}$	$\delta\tilde{t}_{Ar}$
km.	$\frac{\text{torr-liters}}{\text{sec-cm}^2}$	$\frac{\text{torr-liters}}{\text{sec-cm}^2}$	$\frac{\text{torr-liters}}{\text{sec-cm}^2}$
200	$1.91*10^{-13}$	$3.39*10^{-11}$	$6.69*10^{-14}$
300	$1.16*10^{-13}$	$2.04*10^{-12}$	$1.34*10^{-15}$
400	$8.20*10^{-14}$	$2.02*10^{-13}$	$5.02*10^{-17}$
500	$5.98*10^{-14}$	$6.01*10^{-14}$	

These free outgassing rates have been evaluated assuming no adsorption of the gas phase molecules. This is a good assumption as there will be little, if any, adsorption of helium, nitrogen and argon, if gold surfaces are employed.

Outgassing rates for helium, nitrogen and argon have been measured from 304 stainless steel after baking for 12 hours at 300°C (Strausser, 1967). Little evidence of helium or argon outgassing was found. The maximum outgassing rates for helium and argon are thought to be $1x10^{-16}$ torr-liters/sec/cm^2. The outgassing rate for nitrogen is approximately $5x10^{-13}$ torr-liters/sec/cm^2. In comparing the experimental and allowable outgassing rates for helium it appears that the helium outgassing rate does not preclude the proper measurement of helium in the aft cavity. However, it is seen that the nitrogen experimental outgassing rate exceeds the allowable outgassing rate in the aft cavity somewhere between 300 and 400 km. Therefore, the nitrogen outgassing rate should be known if the proper measurement of nitrogen in the aft cavity is to be made at the higher altitudes. The argon experimental outgassing rate also exceeds the allowable outgassing rate in the aft cavity somewhere between 300 and 400 km. However, the experimental argon outgassing rate represents a maximum and could conceivably be lower. Therefore the argon outgassing rate might or might not have to be known to assure the proper measurement of argon in the aft cavity at the higher altitudes.

The free outgassing rates above were calculated assuming a reasonable aft cavity size for configuration 1. In configuration 2, the surface area will be larger but the exit area will be doubled and Figure 6 indicates that the number density ratio of that in the aft cavity to that in the ambient will be equal to or greater than 2.15. Assuming an aft cavity area 10 times as large for configuration 2, the free outgassing rates for configuration 1 should be multiplied by approximately .4 to obtain the free outgassing rates for configuration 2. The same conclusions for free outgassing can be made for configuration 2 as for configuration 1.

The free outgassing rate of a cavity can be investigated while in orbit as well as in the laboratory. If the orifice of the cavity is at an angle of 180° with respect to the free stream vector, a constant number density in the cavity will be obtained. That is, the free outgassing rate is equal to the rate at which the gas is leaving the cavity. This is a good approximation as the amount of gas entering the cavity from the ambient is small because the thermal velocity of the ambient gas is small compared to the satellite velocity. Periodic evaluations of the free outgassing rate should be made while in orbit.

The problem of dynamic outgassing has not been considered in the above discussion. An adsorption equilibrium is thought to be quickly established for helium, nitrogen and argon. However, this equilibrium can be disturbed by turning a filament on as surface desorption would increase due to radiative heating. Equilibrium conditions can also be disturbed by valving as discussed in the Instrument Drift section. These effects should be investigated.

Conclusion

This analysis indicates that the two-gas temperature measurement is feasible and can be successfully employed on a passively stabilized satellite. The use of mass spectrometers to measure two gases with widely different mass numbers replaces the requirement of precise knowledge of the satellite orientation. The low angular rates associated with gravity gradient stabilization do not cause time constant problems in the cavities. Configuration 2 offers the smallest temperature error but the analysis of this configuration is made difficult by its large tubular aft cavity. The temperature error of configuration 1 decreases as the angular separation of the cavities decreases. Although instrument drift will cause an offset in the measured temperature, the variations in the temperature are retained. The correct temperature can be derived, within the limits of instrument calibration and sensitivity, even if the instruments drift if an effective valving system is employed to cross calibrate the instruments. The allowable free outgassing rates of helium and nitrogen appear to be within the state of the art. The temperature accuracy of such a measurement is questionable if the derived temperatures are to be used to study the energy balance and heating in the atmosphere.

REFERENCES

Ballance, J. O., A Monte Carlo program for transmission probability calculations including mass motion, NASA TM-X-53386, 1966.

Bromwell, L. G., Adsorption and friction behavior of minerals in vacuum, M.I.T. Dept. of Civil Engineering, R64-42, 1965.

Brunauer, S., The Adsorption of Gases and Vapors, Physical Adsorption Princeton University Press, I, 1945.

Chizhov, A. F., Temperature measurement of the free atmosphere taking into account the recombinations of atoms, Trudy Tsentral'noy Aerologicheskoy Observajorit, 46, 76-84, 1963, NASA TT-F215.

Clausing, P., Ann. Physik., 12, 961, 1932.

Committee on Space Research, Cospar International Reference Atmosphere 1965, North-Holland Publishing Company, Amsterdam.

de Boer, J. H., The Dynamical Character of Adsorption, Oxford at the Clarendon Press, 1953.

Dushman, S., Scientific Foundations of Vacuum Technique, John Wiley and Sons, Inc., 1962.

Harris, E. L. and G. N. Patterson, Univ. of Toronto Inst. of Aerophys., No. 52, 1958.

Isakov, M. N., Measuring the temperature of the atmosphere with the aid of satellite-borne instruments, Kosmicheskiya Issledovaniya, I, 1963.

Jacchia, L. G., Variations in the earth's upper atmosphere as revealed by satellite drag, Reviews of Modern Phys., 35, 973-991, 1963.

Mark, J. T., Vacuum envelopes for ultra high vacuum systems, RCA Electronic Components and Devices, Power Tube Operations, Lancaster, Penn.

Neir, A. O., J. H. Hoffman, C. Y. Johnson and J. C. Holmes, Neutral constituents of the upper atmosphere: the minor peaks observed in a mass spectrometer, J. Geophys. Res., 69, 4629-4636, 1964.

Newton, G. P., R. Horowitz and W. Priester, Atmospheric density and temperature variations from the Explorer XVII and a further comparison with satellite drag, Planet. Space Sci., 13, 599-616, 1965.

Patterson, G. N., Univ. of Toronto Inst. of Aerophys., No. 41, (revised), 1959.

Repnev, A. I., Trudy Tsentr. Aerol. Inst. 29, 66, 1960.

Smithells, C. J., Gases and Metals, John Wiley and Sons, Inc., 1937.

Stein, J. A. and J. C. G. Walker, Models of the upper atmosphere for a wide range of boundary conditions, J. Atmos. Sci., 22, 11-17, 1965.

Strausser, Y. E., Outgassing measurements of each component of the residual gas released from 304 stainless steel, AVS Meetings, Kansas City, 131-132, 1967.

LIST OF FIGURES

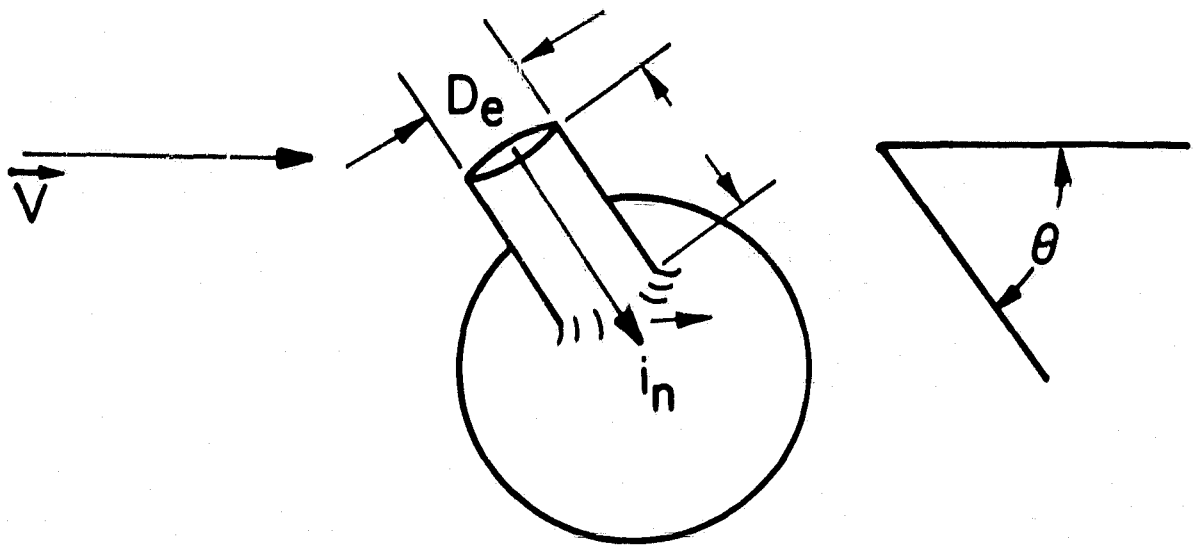

Figure 1. Geometry of simple cavity.

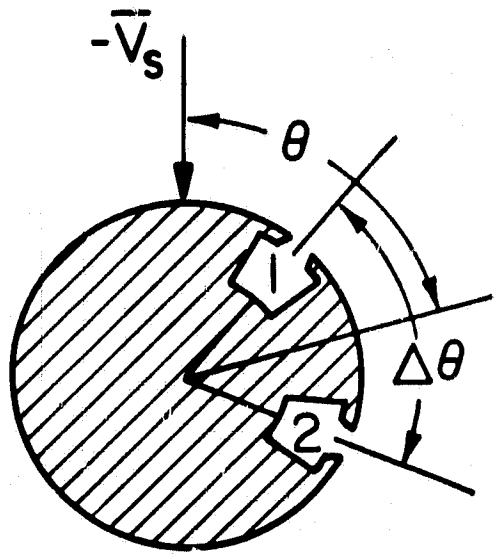

Figure 2. Geometry of Configuration 1.

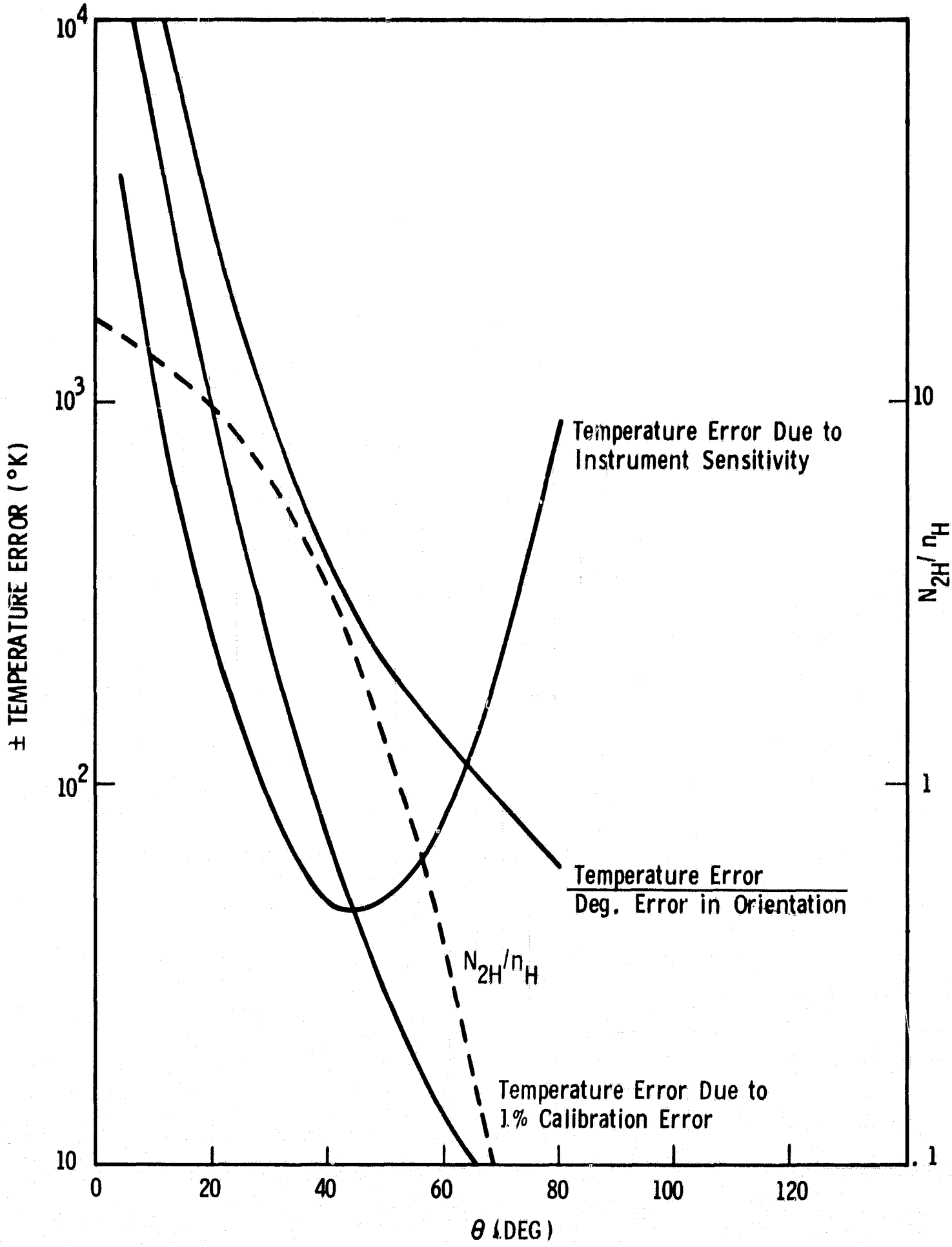

Figure 3. Temperature errors for configuration 1, using helium; $\Delta\theta = 90^{o}$.

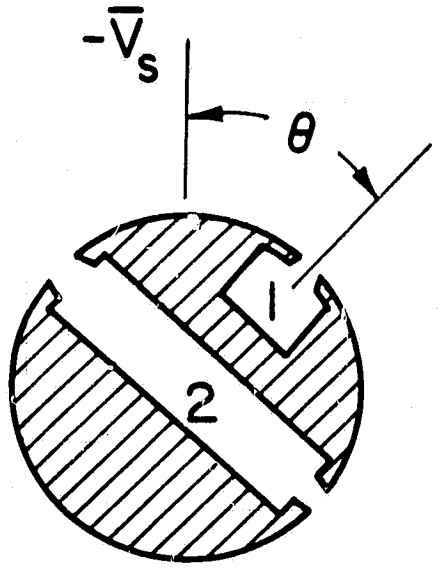

Figure 4. Geometry of Configuration 2.

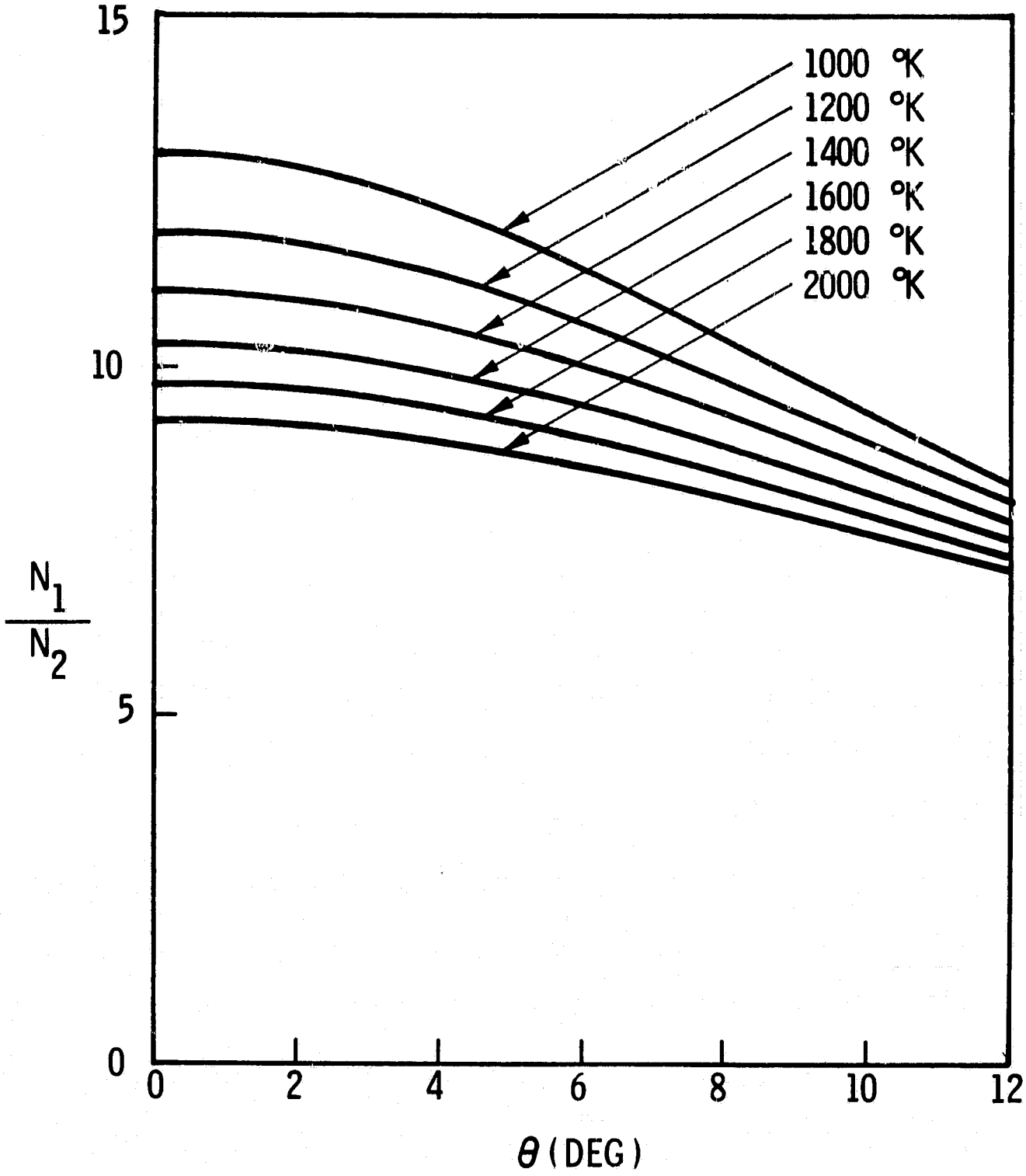

Figure 5. Helium Ratio, R, for Configuration 2.

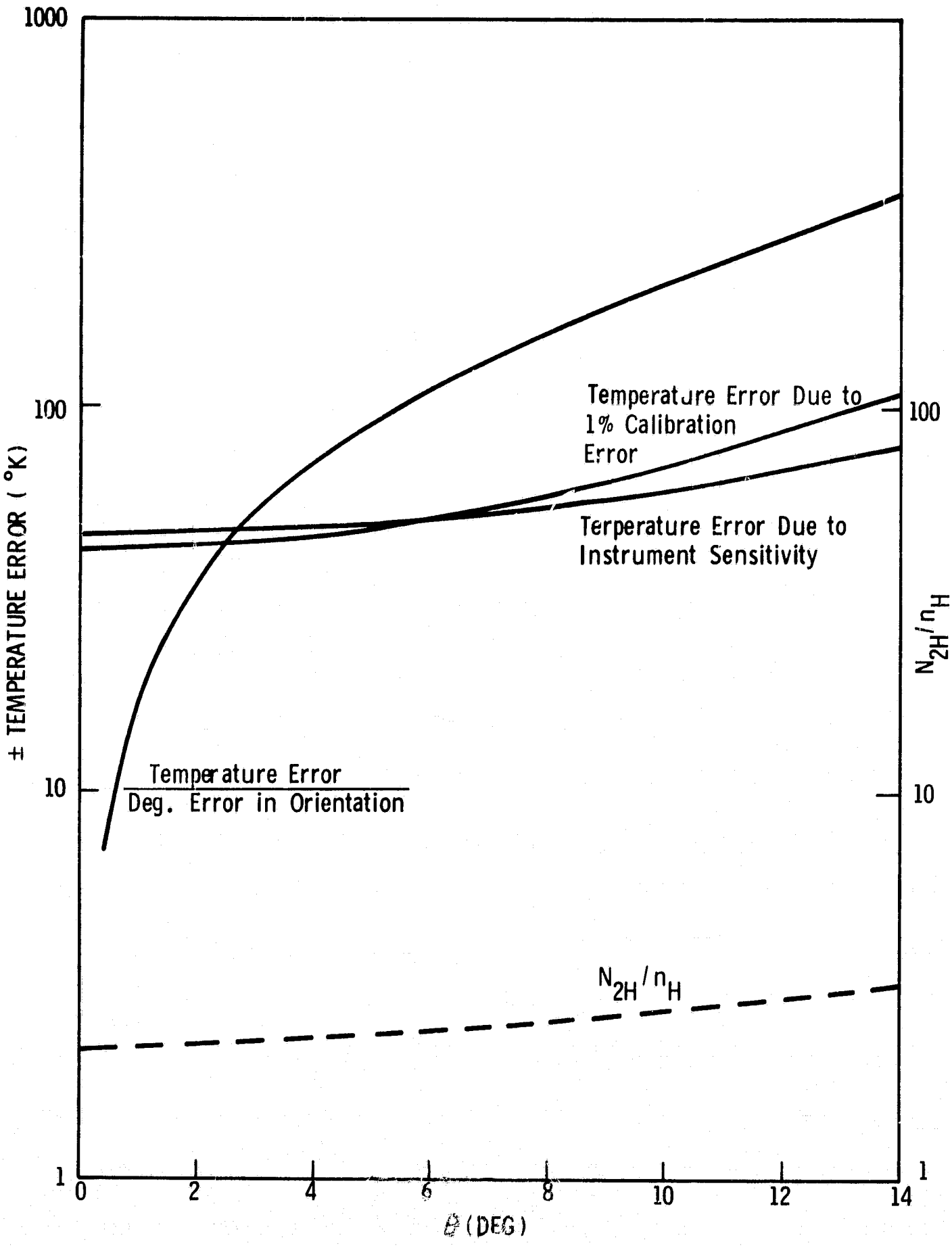

Figure 6. Yaw angle versus orbital time.

Time (orbits)

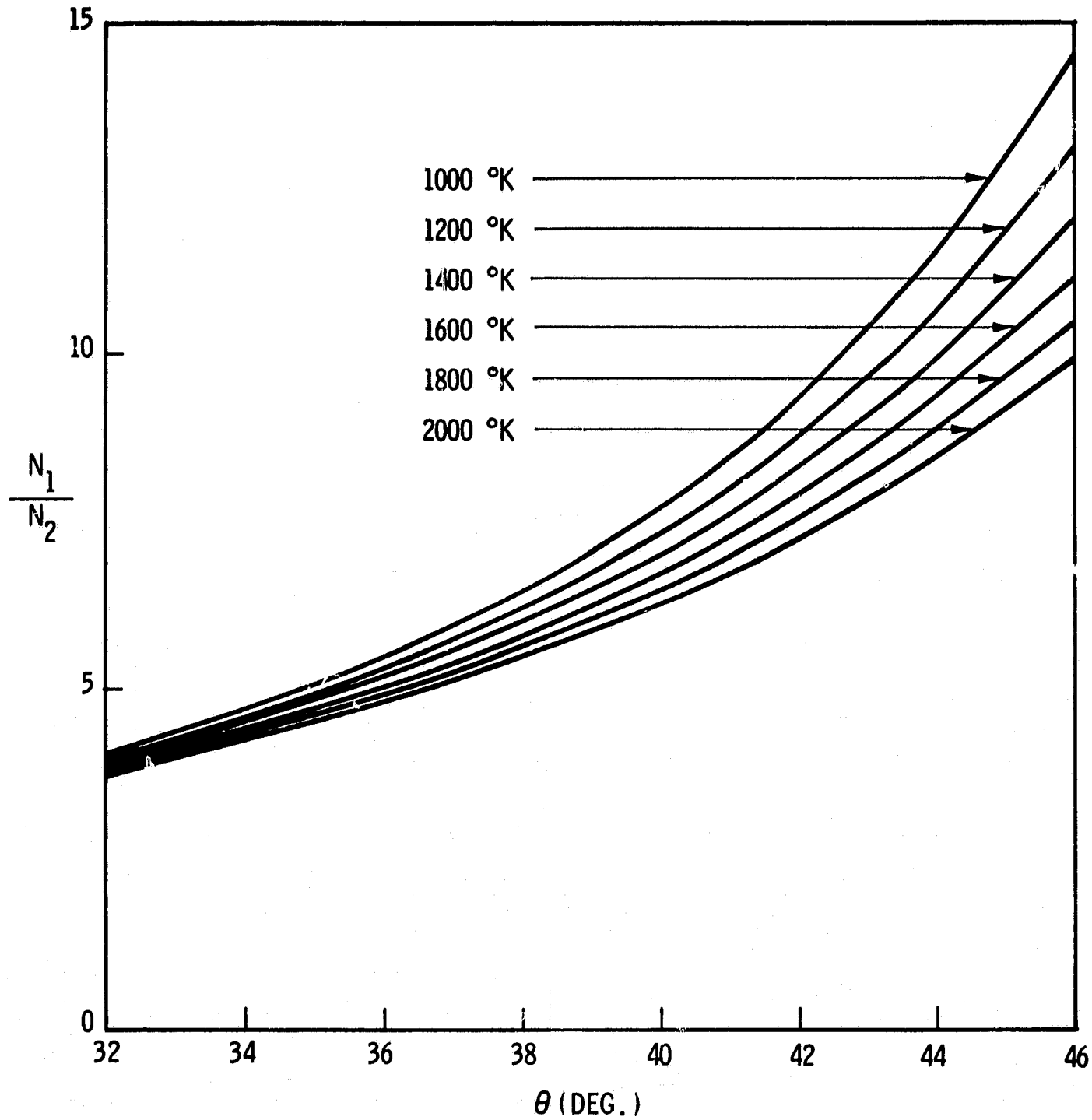

Figure 7. Helium Ratio, R, for Configuration 1; $\Delta\theta = 90^{o}$.

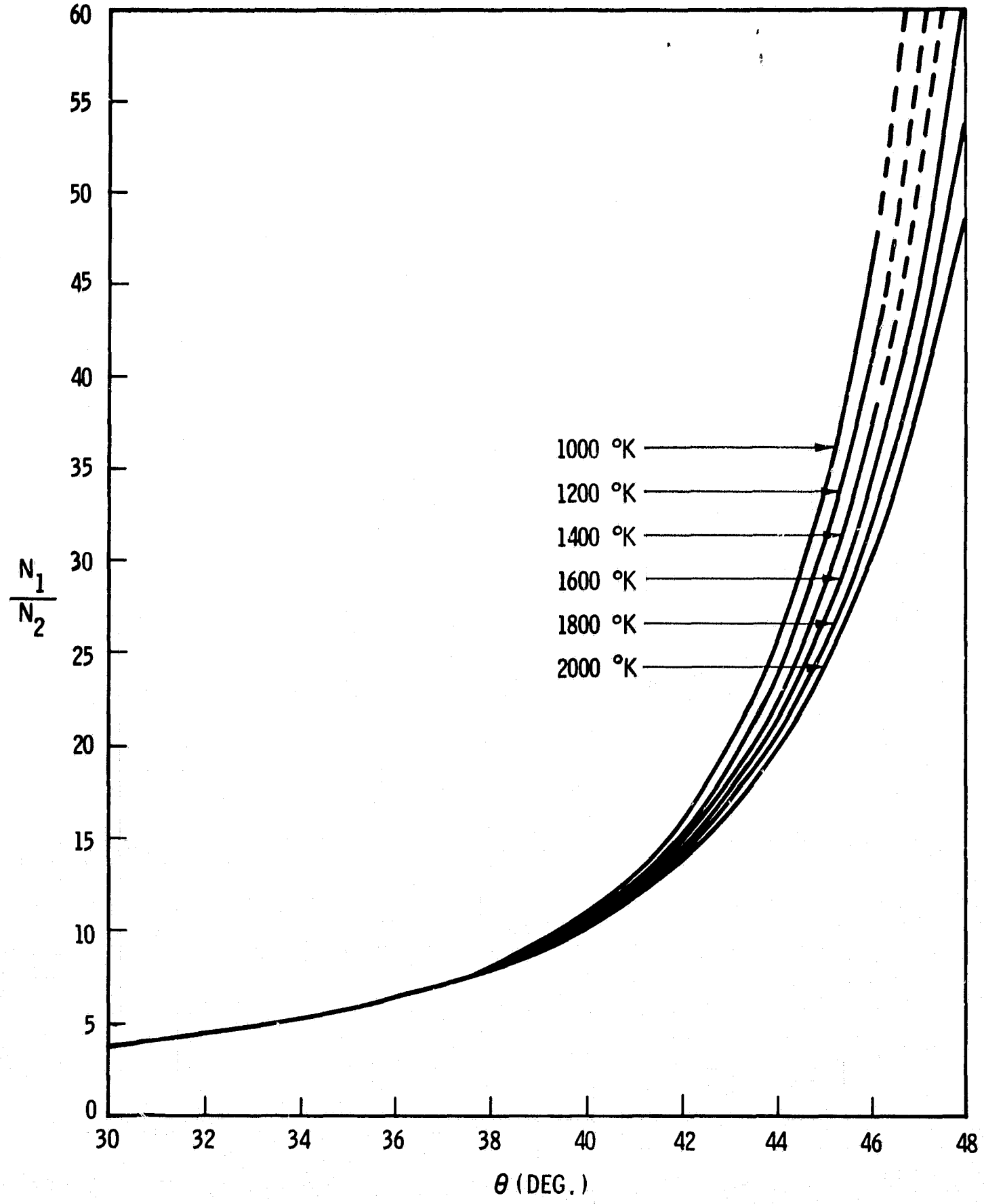

Figure 8. Nitrogen Ratio, R, for Configuration 1;
$\Delta\theta = 90^{o}$

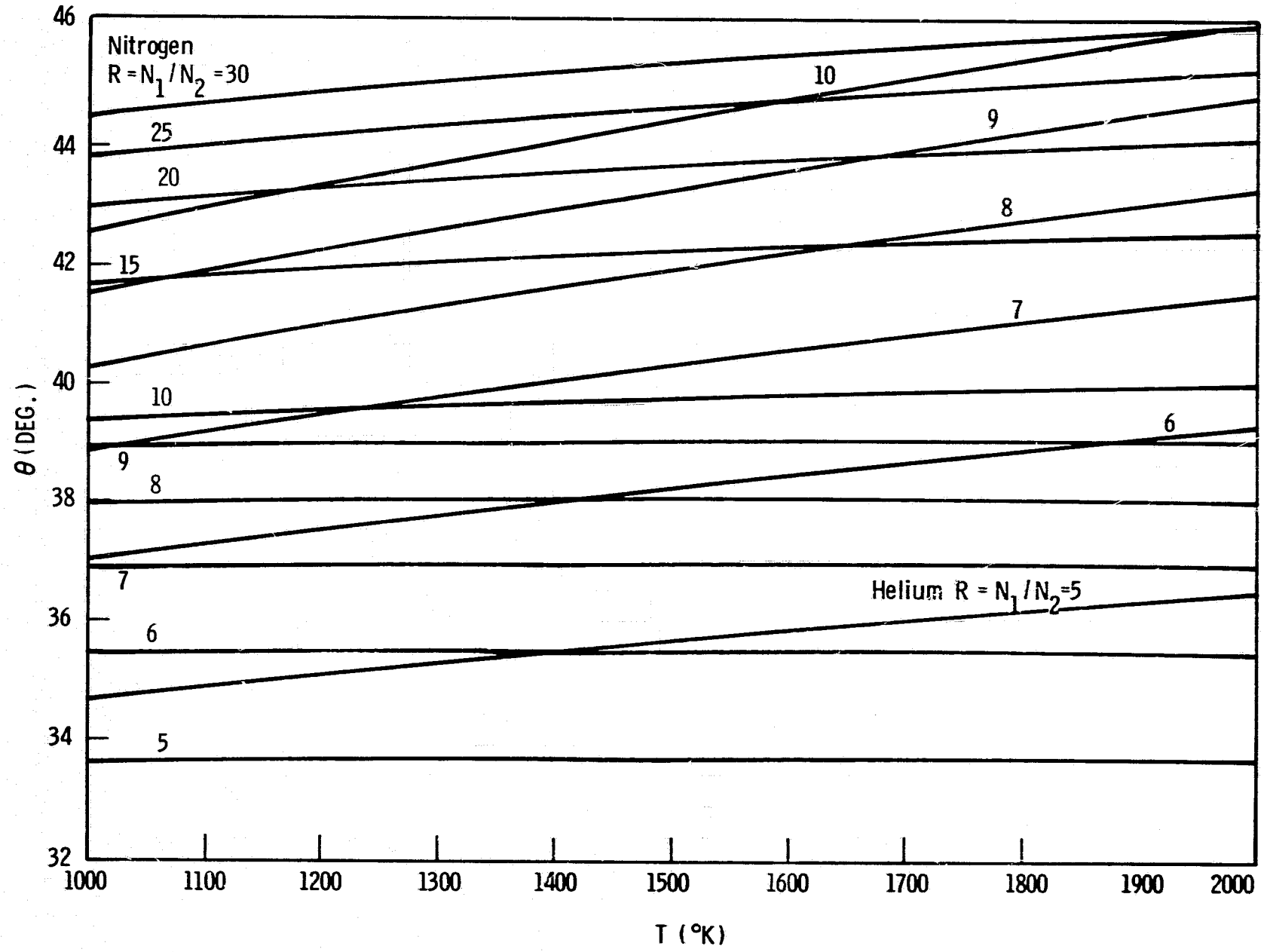

Figure 9. Helium-Nitrogen Temperature Contour for Configuration1: $\Delta\theta = 90^{o}$.

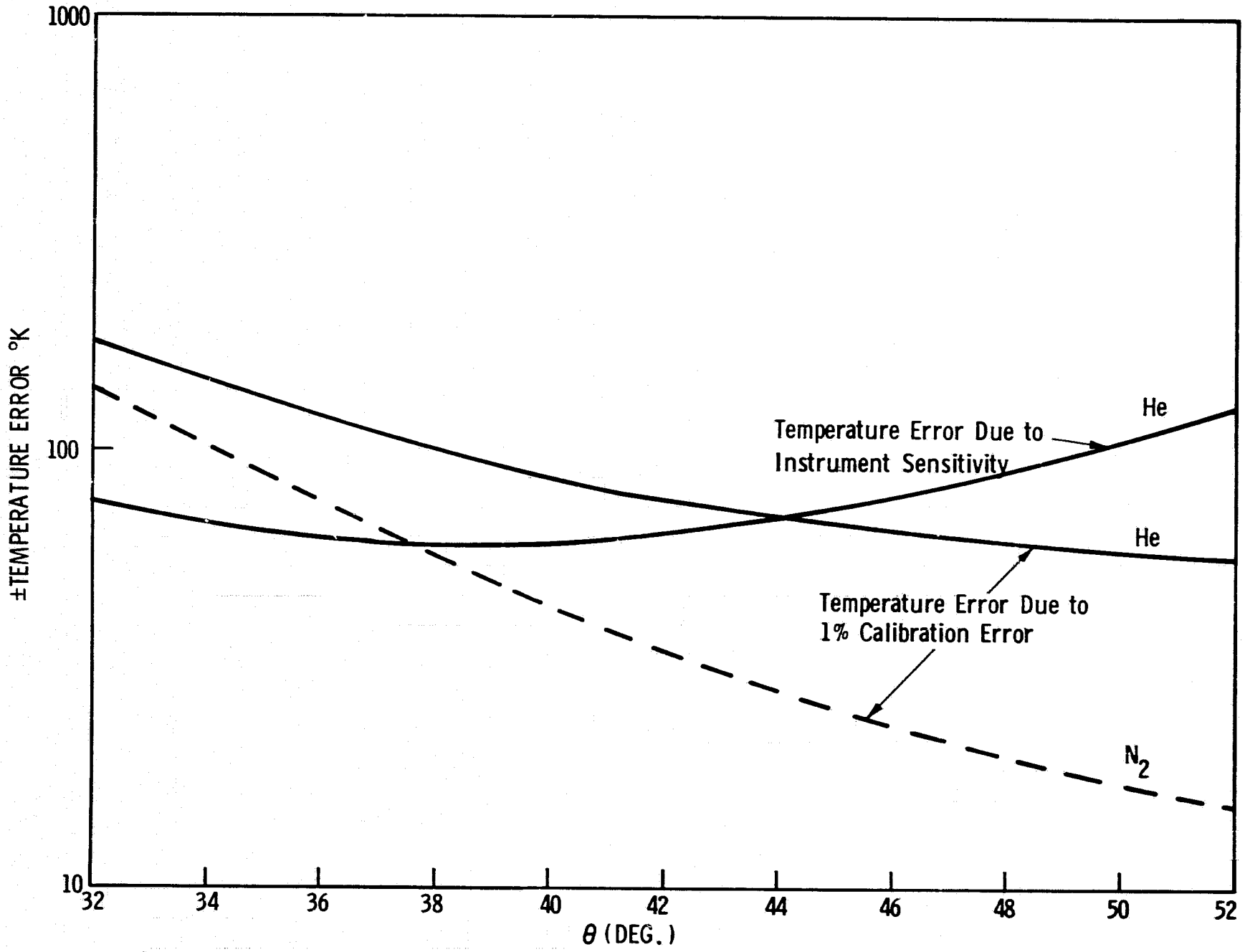

Figure 10. Temperature Errors for Configuration 1 Using Helium and Nitrogen; $\Delta\theta = 90^{o}$.

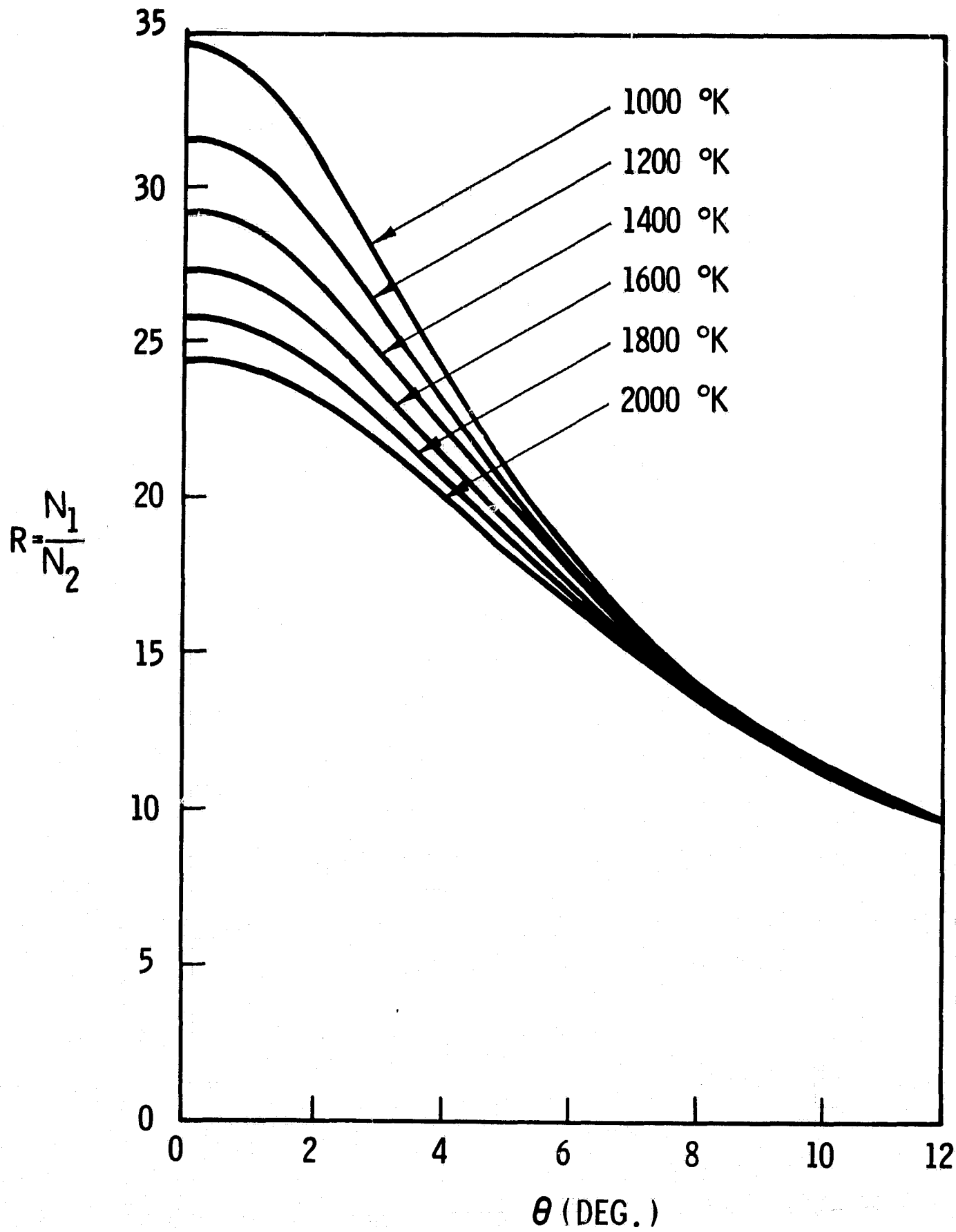

Figure 11. Nitrogen Ratio, R, for Configuration 2.

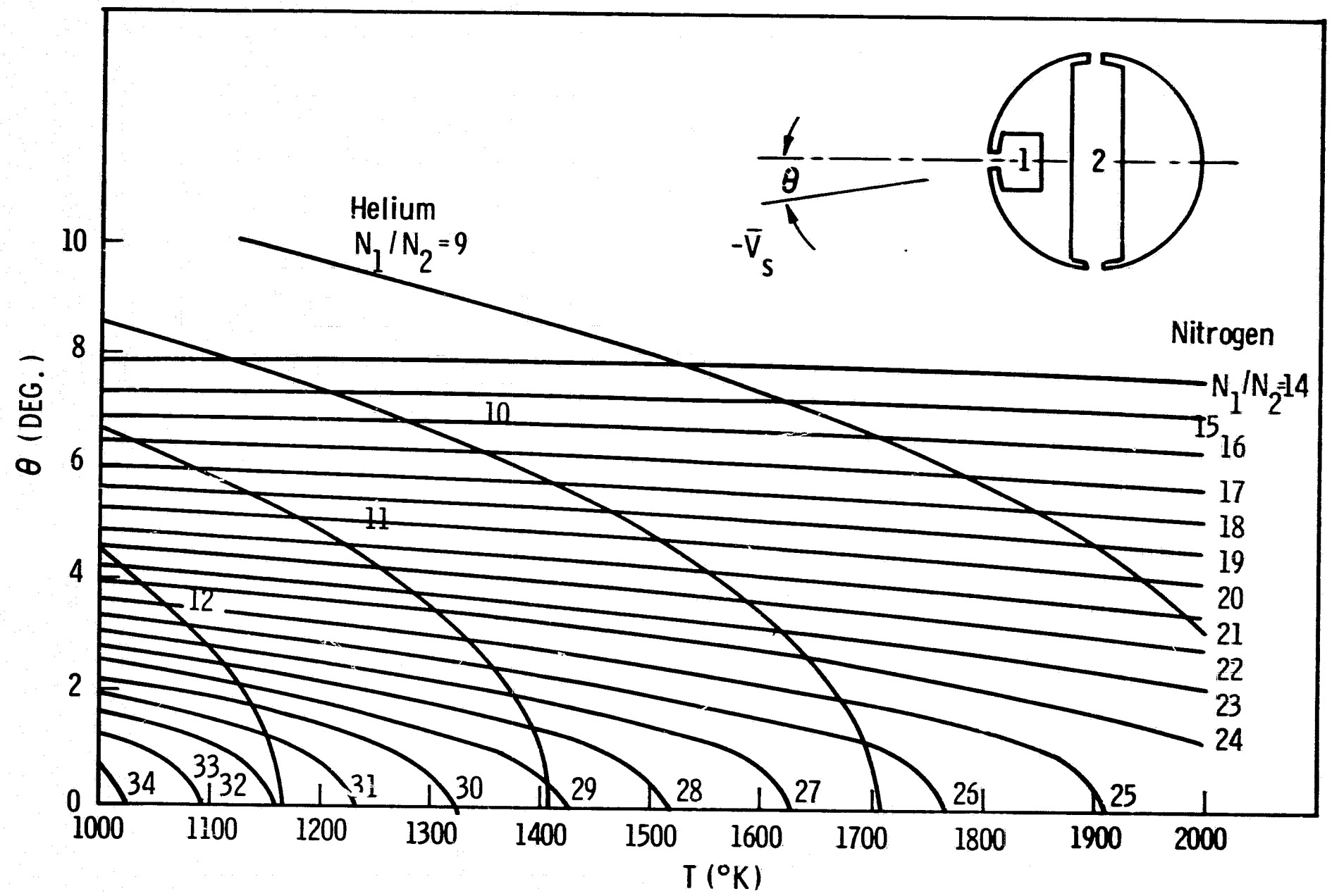

Figure 12. Helium-Nitrogen Temperature Contour for Configuration 2.

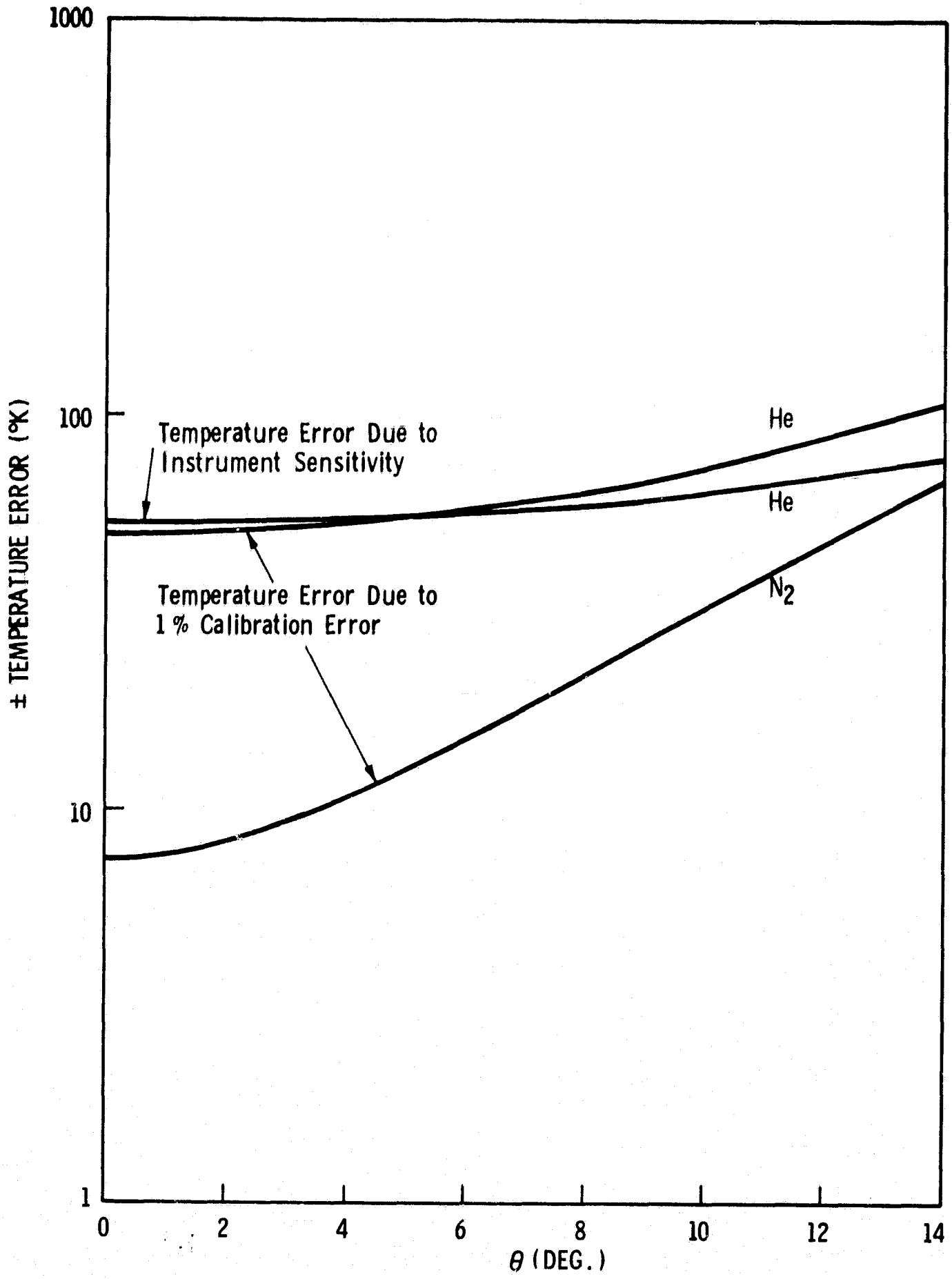

Figure 13. Temperature Errors for Configuration 2 Using Helium and Nitrogen.

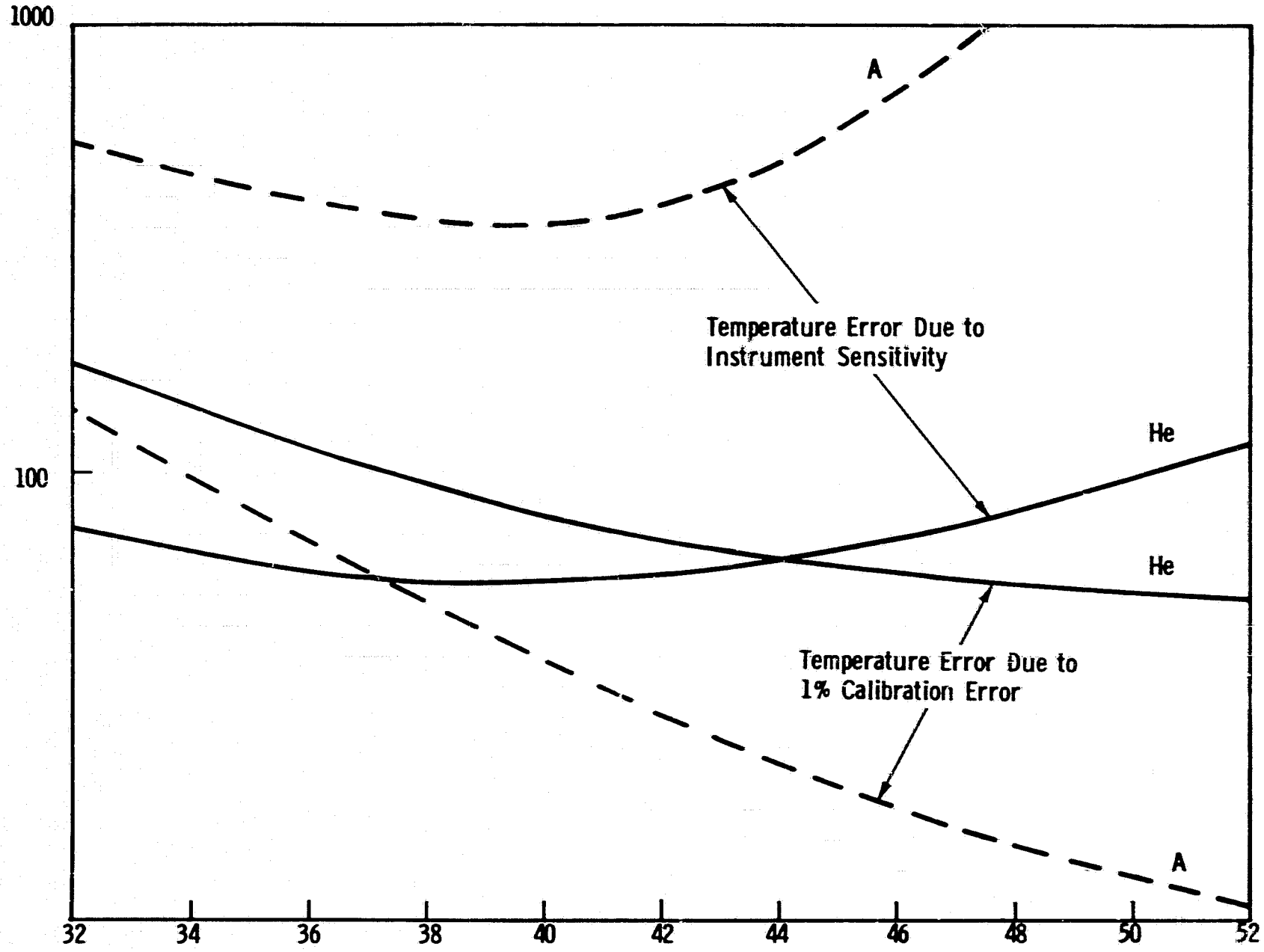

Figure 14. Temperature Errors for Configuration 1 Using Helium and Argon; $\Delta\theta = 90^{o}$.

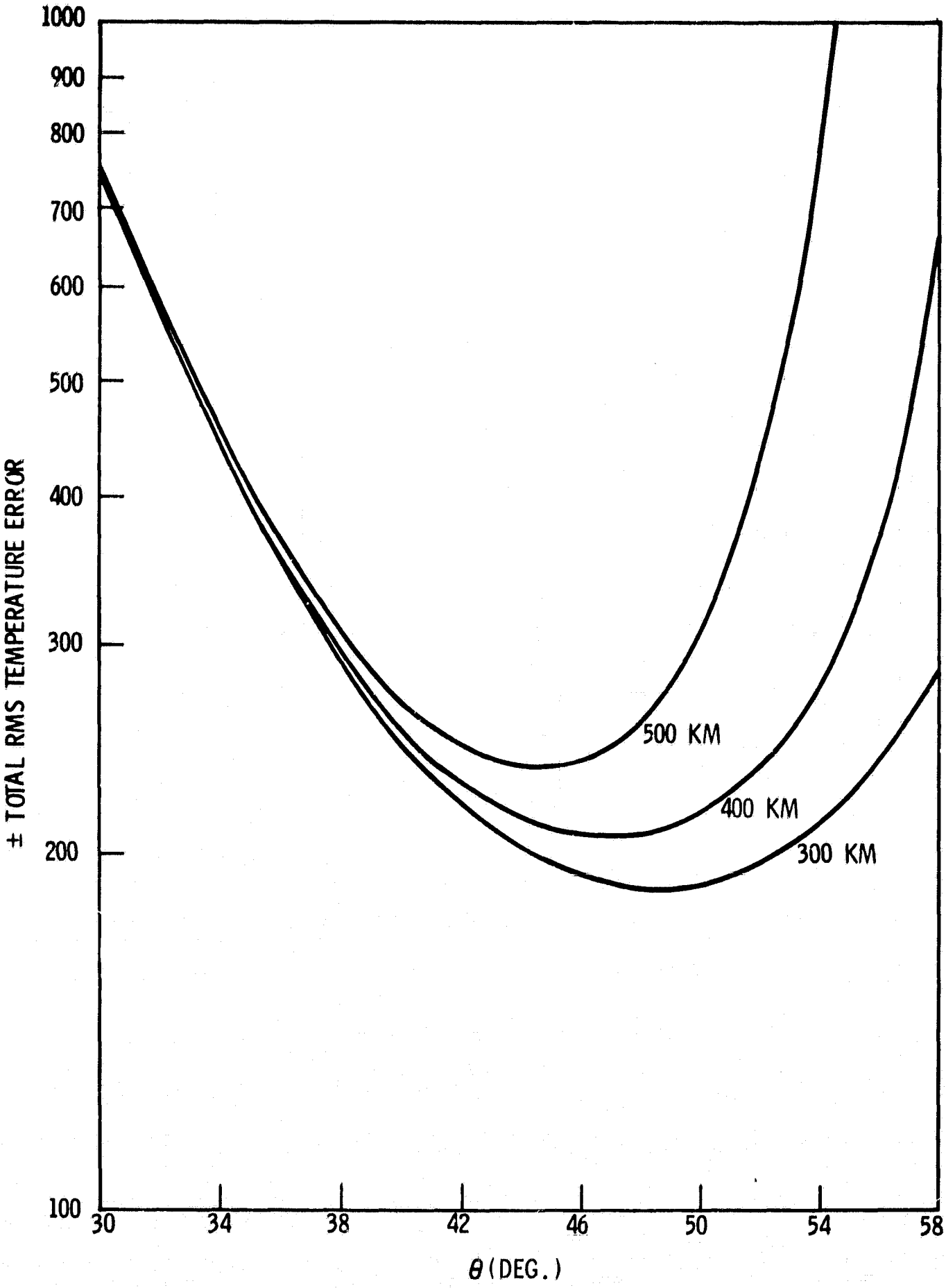

Figure 15. Total RMS temperature error at 300, 400 and 500 km using helium and nitrogen for configuration 1. Instrument calibration error assumed to be 2.5 per cent; sensitivity $1.5 * 10^5$ particles/cm^3; $\Delta\theta = 90^o$.

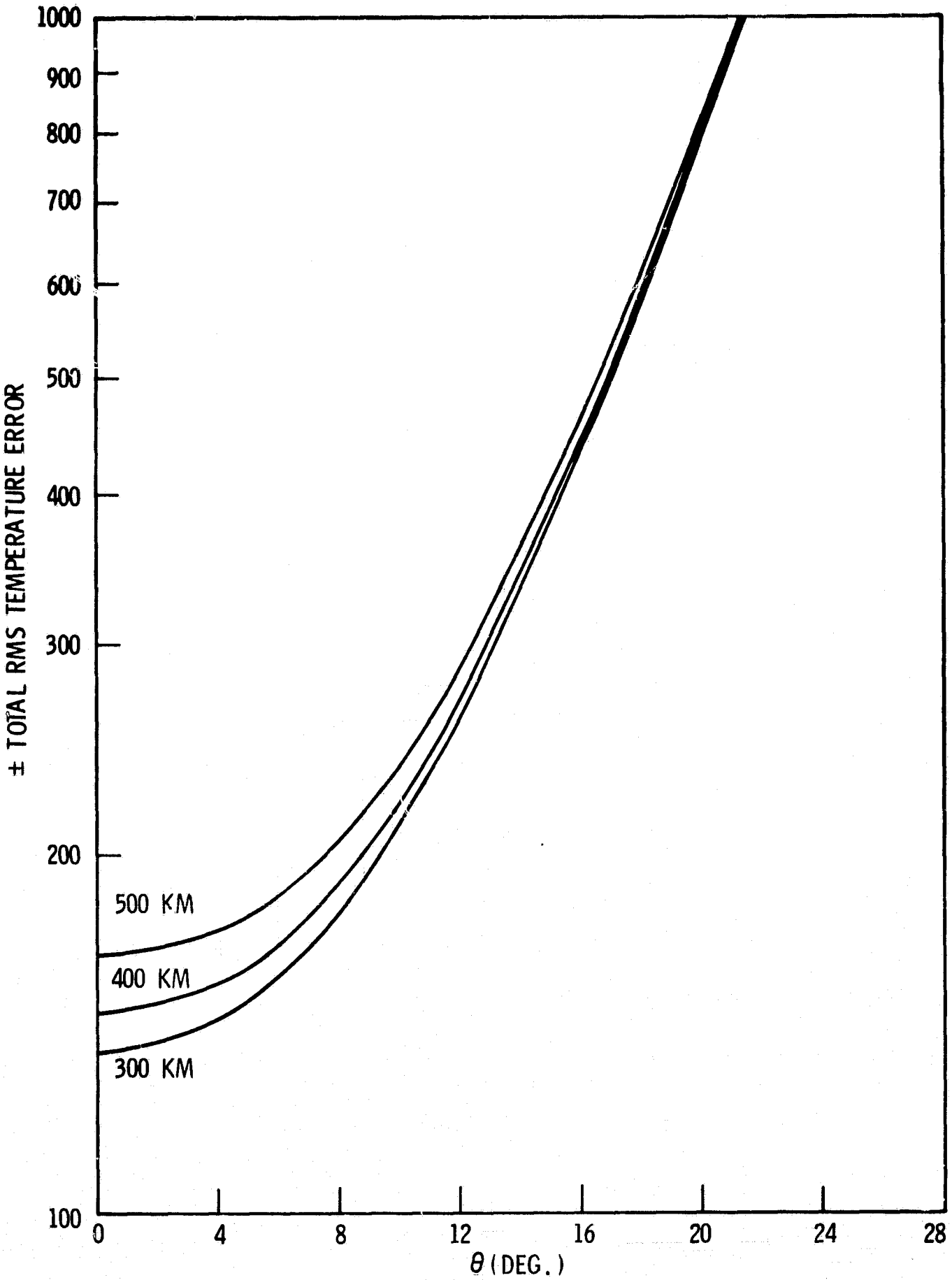

Figure 16. Total RMS temperature error at 300, 400 and 500 km using helium and nitrogen for configuration 2. Instrument calibration error assumed to be 2.5 per cent; sensitivity $1.5 * 10^5$ particles/cm^3.

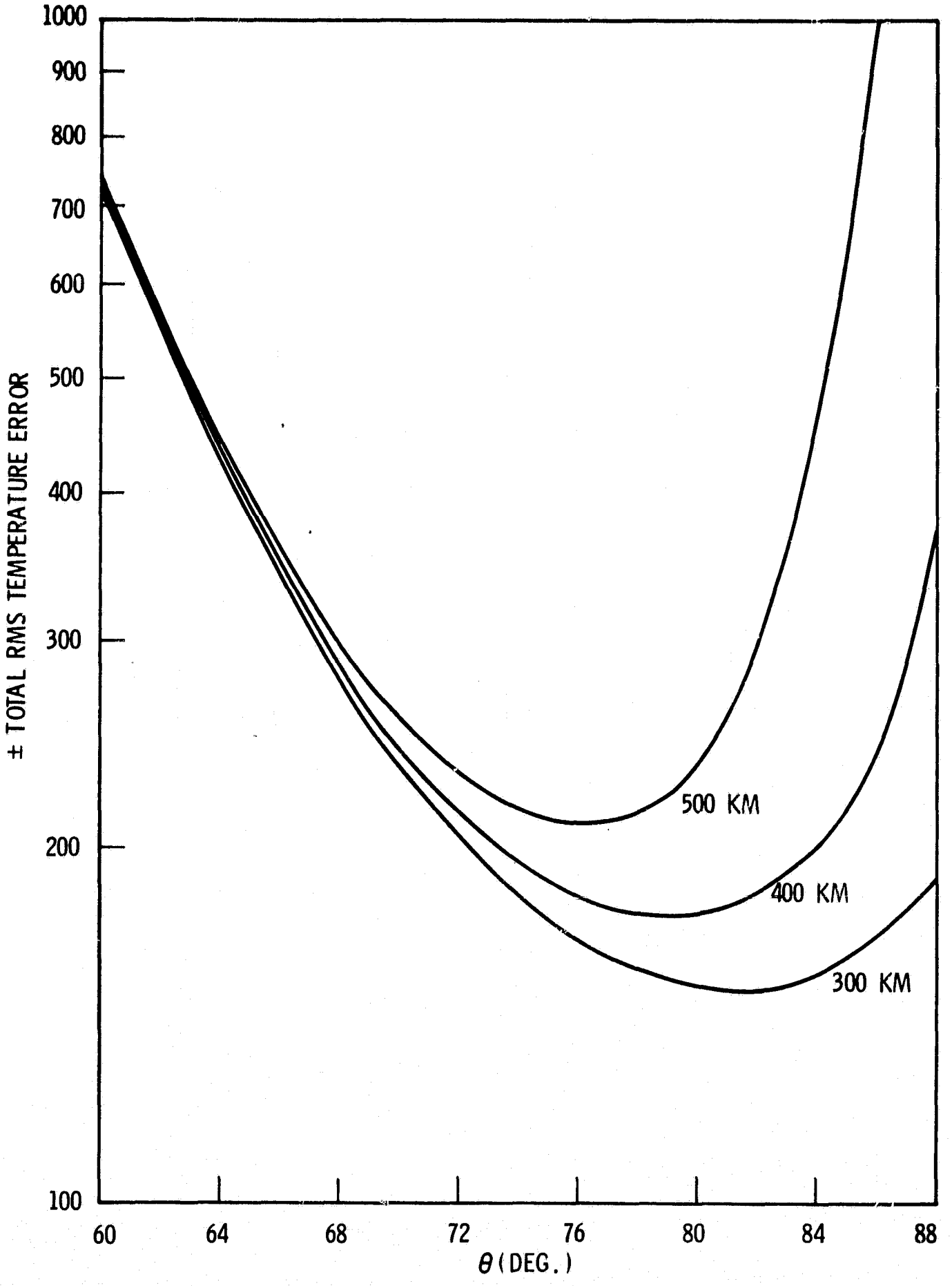

Figure 17. Total RMS temperature error at 300, 400 and 500 km using helium and nitrogen for configuration 1. Instrument calibration error assumed to be 2.5 per cent; sensitivity $1.5 * 10^5$ particles/CM^3; $\Delta\theta = 30^o$.

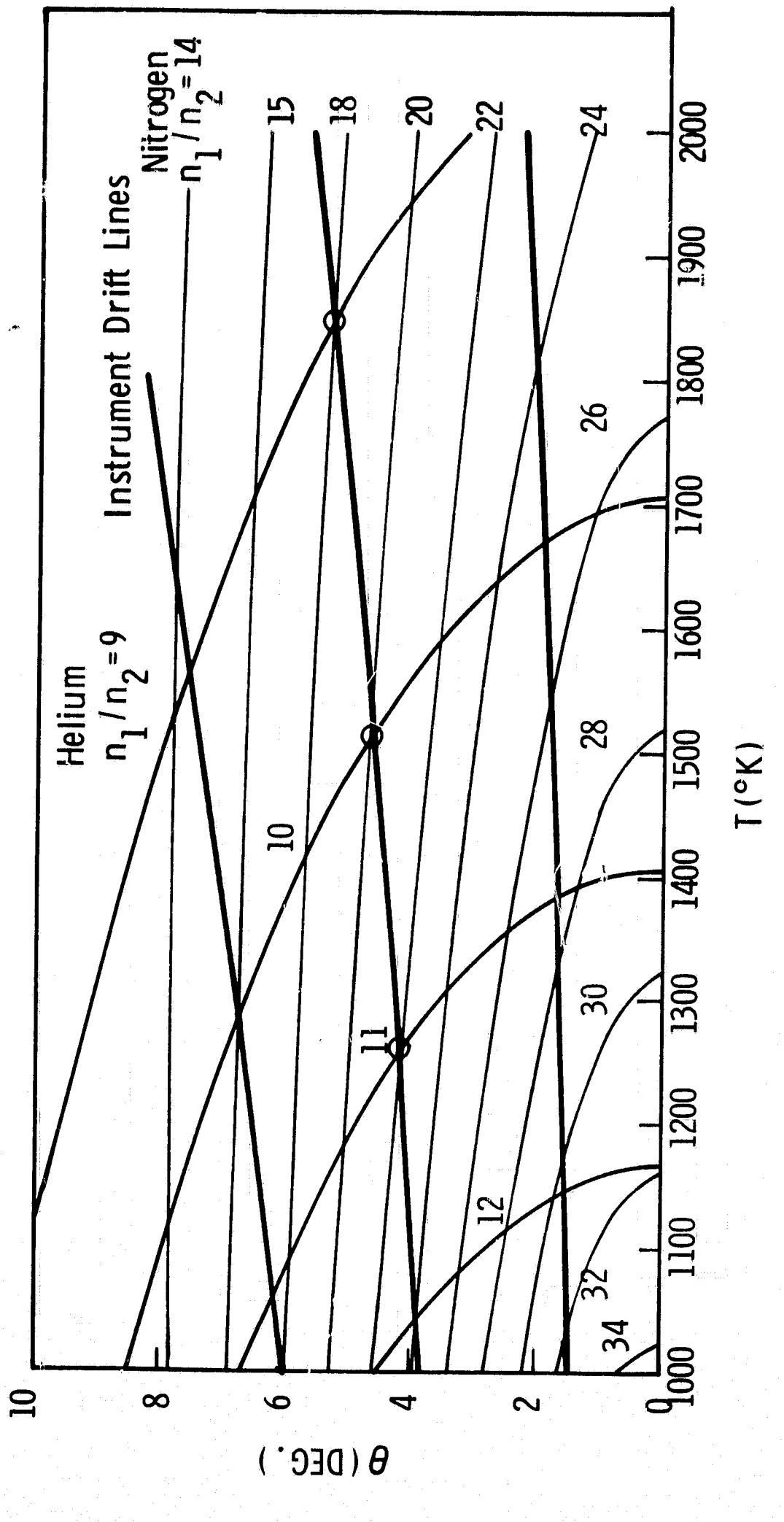

Figure 18. Helium-nitrogen temperature contour for configuration 2 with superimposed instrumental drift lines.

Gas-Surface Interaction Studies

K. D. Mc Watters

Two primary needs to assure meaningful mass spectrometer measurements in a cavity are an evaluation of the free outgassing rates of the cavity surfaces and an understanding of the dynamic adsorption phenomena occuring in a cavity. It has been shown that at an altitude of 300 km, the following free outgassing rates must be achieved if the temperature experiment aboard MICHAEL is to perform properly.

$$\widetilde{\delta t}_{He} = 1.2 * 10^{-13}$$

$$\widetilde{\delta t}_{N_2} = 2 * 10^{-12} \qquad \frac{\text{Torr-liters}}{\text{sec-cm}^2}$$

$$\widetilde{\delta t}_{AR} = 1.3 * 10^{-15}$$

Equilibrium conditions in a cavity can be drastically changed by turning a filament on or valving as discussed in the instrument drift section. The need to approach these problems experimentally was apparent due to the lack of theory in this area.

Experimental equipment was purchased to carry out the experiments. The main items required in this experimental setup was a MAT AMP-3 quadrupole mass spectrometer and a VI-321 Varian Ultra High Vacuum System capable of obtaining the pressures required. The free outgassing rates are to be measured in a 304 stainless steel cavity attached to the main vacuum chamber, as shown in the figure.

The general equation relating the pressure in the cavity to that in the chamber is

$$\frac{V_1 dP_{n_1}}{dt} + C P_{n_1} = C P_{n_2} + Q_{s_n}(t)$$

Where

P_{n_1} = pressure of n^{th} species in cavity

P_{n_2} = pressure of n^{th} species in chamber

V_1 = volume of cavity

C = conductance of orifice

$Q_{s_n}(t)$ = outgassing rate of n^{th} species

$Q_{s_n}(t)$ may be represented by:

$$Q_{s_n}(t) = \delta\tilde{t}_n A - P_{n_1} f_n e_n A$$

where

$\delta\tilde{t}_n$ = free outgassing rate in torr-liters/ $sec\text{-}cm^2$ for n^{th} species

A = surface area of cavity

f_n = effusion law factor

e_n = sticking coefficient

Therefore

$$Q_{s_n}(t) = \delta\tilde{t}_n A - P_{n_1} f_n e_n A = V_1 \frac{dP_{n_1}}{dt} - CP_{n_2} + CP_{n_1}$$

The problem is to evaluate the free outgassing rate, $\delta\tilde{t}_n$, which is defined as the outgassing from and through the surface.

$$\delta\tilde{t}_n A = V_1 \frac{dP_{n_1}}{dt} + CP_{n_1} - CP_{n_2} + P_{n_1} f_n e_n A$$

The sticking coefficient (e_n) is very small for helium, argon and nitrogen at the pressures at which we will be working. There will be little, if any, adsorption of gases with adsorption energies less than 15 Kcal/mole below 10^{-4} torr at room temperature. Therefore the last term of the above equation can be neglected. That is, there is no adsorption of the argon, helium, and nitrogen gas phase molecules.

$$\delta \tilde{t}_n A = V_1 \frac{dP_{n_1}}{dt} + C P_{n_1} - C P_{n_2}$$

One obvious way to measure $\delta \tilde{t}_n$ is to wait until an equilibrium condition is achieved. That is let $\left(\frac{d P_{n_1}}{dt}\right) \to 0$

then

$$\delta \tilde{t}_n A = C P_{n_1} - C P_{n_2}$$

What must the partial pressures of helium, nitrogen and argon be in the chamber if one can neglect the flux of particles into the cavity. This calculation will be made on the basis of the outgassing rates at 300 km which must be achieved if the temperature experiment is to work. One must also assume a cavity area and orifice diameter. The object of this study is to determine the lowest outgassing rates of stainless steel. This, by necessity, is difficult as an ion source must be placed inside the cavity. The ion source contains eight (8) different types of material. Therefore, it would be desirable to have a large ratio of cavity area to ion source surface area if the free outgassing rate is to be related to stainless steel. However it would be desirable to simulate a flight model of the cavity when dynamic adsorption experiments are conducted. Therefore, one faces a compromise when specifying the proper size of the cavity. A cavity with a surface area of 600 cm^2 will be assumed for the calculations. The orifice diameter is assumed to be 1 cm. The conductance of the orifice is given by;

$$C = 3.64\, A\sqrt{\left(\frac{T}{M}\right)} \quad \frac{\text{liters}}{\text{sec}}$$

Let $T = 300^{o}\ K$

$A = \pi/4$

Therefore

$$C = \frac{49.6}{(M)^{\frac{1}{2}}} \quad \frac{\text{liters}}{\text{sec}}$$

What pressure is required in the cavity such that the flow out of the cavity is equal to the free outgassing rate?

$$P_{n_1} = \delta \tilde{t}_n \, A/C$$

$$P_{He_1} = \frac{1.2 \times 10^{-13} \times 600}{24.8}$$

$$P_{He_1} = 2.9 \times 10^{-12} \text{ torr}$$

$$P_{N_1} = 1.28 \times 10^{-10} \text{ torr}$$

$$P_{AR_1} = 9.94 \times 10^{-14} \text{ torr}$$

In order to neglect the flow of gas into the cavity the partial pressures in the chamber should be 1% of those in the cavity.

$$P_{He_2} = 2.9 \times 10^{-14} \text{torr}$$

$$P_{N_2} = 1.28 * 10^{-12} \text{torr}$$

$$P_{AR} = 9.94 \times 10^{-16} \text{ torr}$$

These chamber partial pressures would be hard to obtain. The partial pressures of helium and nitrogen could possibly be achieved if the total pressure in the chamber was in the 10^{-12} torr range. However, it is not necessary to

achieve these low pressures. One can still evaluate the free outgassing rate without neglecting the flow of gas into the cavity. For this type of calculation a residual gas analysis must be obtained for the chamber at various total pressures. Every effort should be made to achieve the lowest partial pressures in the chamber such that the ratio, P_{n_1}/P_{n_2}, will be high.

One source of gas which has not been accounted for in the equations is the backstreaming from the spectrometer. The spectrometer, as received, has a large conductance between the rod section and the ion source. This will have to be closed, leaving the 1 mm diameter orifice through which the ions are accelerated. One must therefore evaluate the backstreaming through this 1mm diameter orifice. The conductance of this orifice is;

$$C_s = \frac{.496}{(M)^{\frac{1}{2}}} \quad \frac{\text{liters}}{\text{sec}}$$

What pressure in the analyzing section must one have to be assured that the flux coming from the analyzing section is 1% of that coming from the walls ?

$$.01\ \delta\tilde{t}_n A = P_{n_s} C_s \quad \frac{\text{torr liters}}{\text{sec}}$$

$$P_{n_s} = \frac{.01\ \delta\tilde{t}_n\ A}{C_s}$$

Using the free outgassing rates which must be achieved at 300 KM, the partial pressures in the analyzing section should be;

$$P_{He_s} = 2.9 * 10^{-12} \text{ torr}$$
$$P_{N_s} = 1.28 * 10^{-10} \text{ torr}$$
$$P_{AR_s} = 9.94 * 10^{-14} \text{ torr}$$

These are the partial pressures in the analyzing section which should be achieved if one is to neglect the flux from the analyzing section. It is therefore mandatory that the analyzing section be pumped separately to reach these pressures. A total pressure in the 10^{-10} torr range should be sufficient to provide the required partial pressures for helium and nitrogen. The desired partial pressure of argon in the analyzing section would be difficult to achieve.

Another method to evaluate the free outgassing rate is to simply close the 1 cm orifice. The resulting equation to be studied is:

$$\delta \tilde{t}_n A = V_1 \frac{dP_{n_1}}{dt}$$

The change of pressure with time can then be observed in order to calculate the free outgassing rates. This equation assumes no input into the cavity. Again, the flux of gas from he analyzing section must be small enough to neglect.

The measurement of the nitrogen free outgassing rate is made difficult by the evolution of CO. A cracking pattern analysis must be performed in order to differentiate between N_2 and CO.

Dynamic absorption studies will also be carried out in the cavity. The effect of turning a filament on in the cavity will be observed and the time required to reach an equilibrium pressure will be measured. A mass analysis will be made of the gas desorption due to the radiative heating of the walls by the filament. The effect of this gas desorption will be studied versus surface treatment. The effects of induced outgassing will be measured. This will be achieved by closing orifice C and leaking in a specific gas into the vacuum chamber. The orifice C will then be opened and the cavity will experience a step function in pressure. A mass analysis will be made of the induced gas desorption. The effect of using different gases as well as surface treatment of the cavity will be studied.

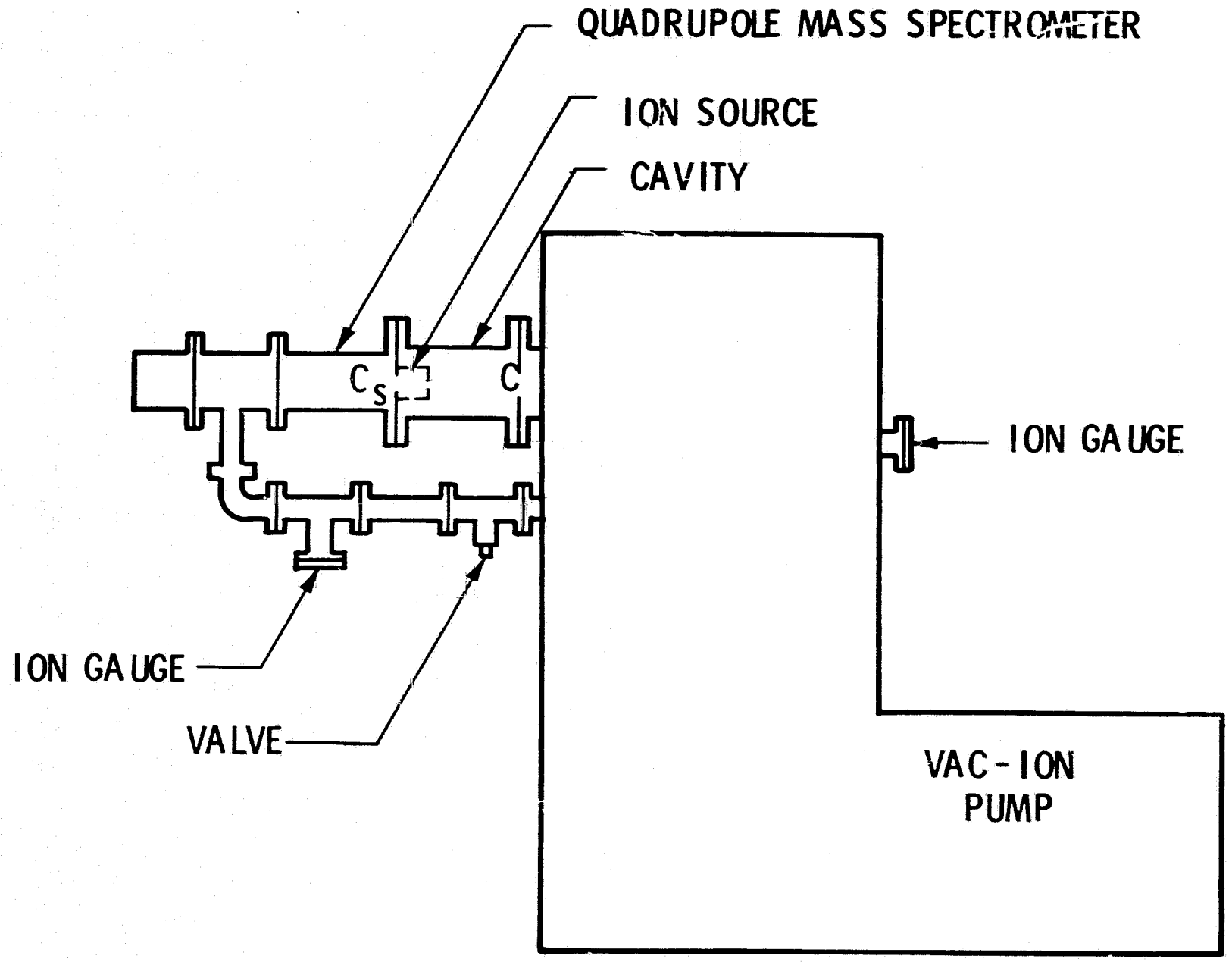
QUADRUPOLE MASS SPECTROMETER
ION SOURCE
CAVITY
C_s
C
ION GAUGE
ION GAUGE
VALVE
VAC-ION
PUMP

Figure 1

Hyberbolic Ion Source

K. D. Mc Watters

The need for a clean, low power ion source is a necessity for satellite mass spectrometer applications. It was felt that a hyperbolic ion source as shown in Figure 1 could be adapted to provide these characteristics. Such an ion source was constructed and tested. The electrons and ions are accelerated by the electric field generated by the hyperbolic body, the filament plate, and the bottom cap. The mechanism of operation can be described briefly as follows: the filament plate and the bottom cap are held at ground potential and the hyperbolic body at a positive voltage, say +80 volts. The filament is also run at a positive voltage but less than the body voltage, say +30 volts. Therefore, an electron coming off the filament accelerates toward the hyperbolic body. Ions created in the upper half of the ion source accelerate toward the filament plate and are neutralized. A sufficient number of electrons accelerate into the lower half of the ion source so that the ions formed by these electrons accelerate toward the bottom cap. . The ions are then collected on the collector after passing thru the orifice in the bottom cap. One very important feature of the source is its ability to focus. The dotted line in Figure 1 represents the volume in which an ion, once formed, will be focused into the orifice. This feature is most important when the necessity for a low power ion source is considered. In an effort to increase the efficiency of the ion source

a magnetic field of 100 gauss was applied along the ion source axis. The electrons are now forced into a spiraling motion and will move up and down the ion source axis. Under optimum conditions a collection current of 3.1×10^{-10} amps was obtained at a pressure of 1×10^{-6} torr and at an emission current of 0.1 μ amp. Upon comparing this current with another laboratory ion source and making appropriate corrections for different size extraction orifices, it is safe to say that there is a decrease by a factor of 1000 in the emission current required in the hyperbolic ion source in order to obtain the same collection current as measured by the other laboratory ion source. This factor represents a considerable savings in power usage if the hyperbolic ion source is to be used in a satellite application.

The device has been troubled by a moding problem which may be due to charge build up on the surfaces. The source was made of aluminum and was susceptible to charge build up on the oxide layer formed on the aluminum. This problem could be solved if proper surfaces were employed. The moding problem could also be caused by the Barkhausen effect wherein the electrons pick up sufficient energy from the magnetic field to reach the collector. This problem might be solved by tilting the axis of the magnetic field slightly with respect to the ion source axis. This would tend to remove the electrons at such a rate that they would not acquire the energy necessary to reach the collector.

In conclusion, the hyperbolic ion source offers a significant advantage over our present laboratory ion source in terms of power required to obtain the same collection current. The hyperbolic ion source is troubled by moding problems but it appears that techniques are available to eliminate them.

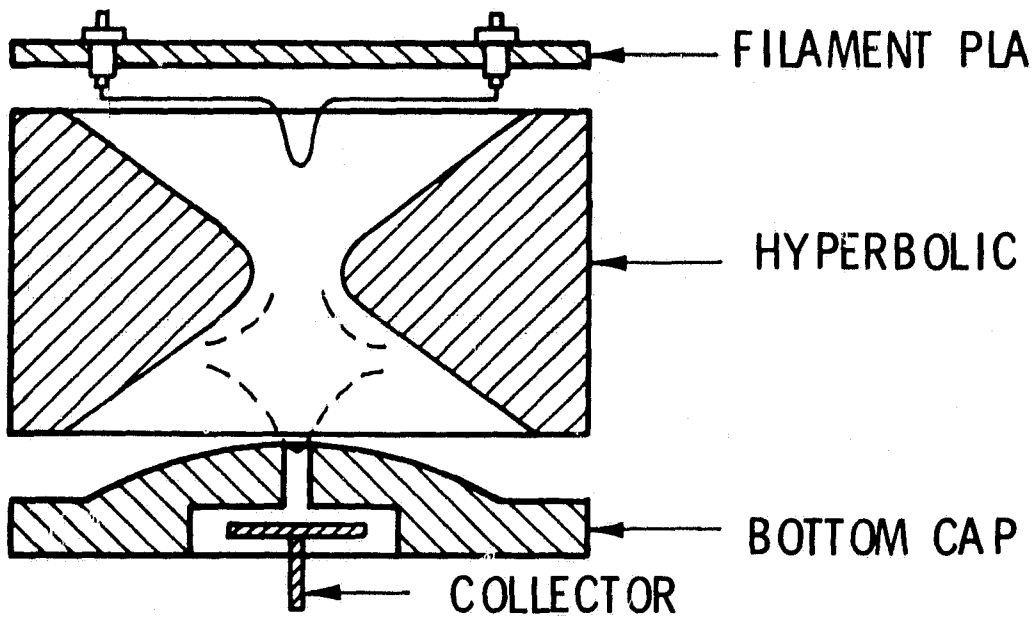

Figure 1

The Motion of a Three Body Satellite Under the Action of Gravitational and Magnetic Torques.

G. Bonfanti

Abstract

The equations of motion of a gravity-gradient satellite under the action of gravitational and magnetic torques are derived. The satellite consists of a main body and two smaller masses connected to it by extensible rods assumed rigid in bending but not in torsion. The damping of the system is provided by two magnetically anchored dampers contained in the two small masses.

The motions of the satellite in the orbit will be controlled by magnetic torques generated by the interaction of an induced magnetic flux and the earth magnetic field. Conclusions on the feasibility of this control scheme are presented.

Introduction.

The basic configuration analyzed in this paper is that of a gravity-gradient satellite consisting of a central or main body, containing the experimental package per se, to which two smaller masses are symmetrically connected by means of extensible rods. These rods are assumed rigid in bending but not in torsion. Each of the two smaller or end masses contains a magnetically anchored viscous fluid damper designed and tested by General Electric. Basically these dampers consist of an outer sphere fixed at the end of the extensible rods, and containing a smaller sphere with a bar magnet which follows the earth magnetic lines. The gap between the two spheres is fitted with a viscous fluid which serves as the damper of the relative motion between the two spheres. Obviously this relative motion is due to the fact that the outer sphere is connected to the satellite by the extensible rod, while the inner sphere is fixed on the earth magnetic lines.

The equations of motion are derived following the approach of reference 2 and were programmed for solution on high speed computers.

Because of the nature of the experiments that the University of Michigan intends to carry on board a satellite of the same configuration as analyzed in this paper, it became apparent that at times it would be desirable to fly the satellite at a yaw orientation different from that attained after the satellite had stabilized on its orbit. It could be advantageous to fly forming a given angle with the free stream velocity, or perhaps even yaw the satellite 180^{o} and maintain this orientation for a given period of time. To achieve these maneuvers, external torques have to be supplied by some means that would not contaminate the environment. This eliminates thrusters.

Mr. H. F. Schulte of the University of Michigan, High Altitude Engineering Laboratory suggested that the needed torques be produced by the interaction of an induced magnetic field and the earth's magnetic fields. The feasibility of this method was investigated. The equations describing the resulting control torques are derived in Section 6. The method seems to be adequate and feasible.

1. Equations of motion.

The satellite will be assumed to be composed of three rigid bodies: a mass m_1 with two massless rigid rods with center of mass at a distance $\bar{r}_1$, from O (Fig. 1) and two masses m_2 and m_3, hinged one at each end of the two rods. The center of mass of each of these two masses will be at a distance $\bar{r}_2$ and $\bar{r}_3$ from O respectively. The center of mass of the system will be at distance $\bar{r}$ from O where O is located at the center of the earth.

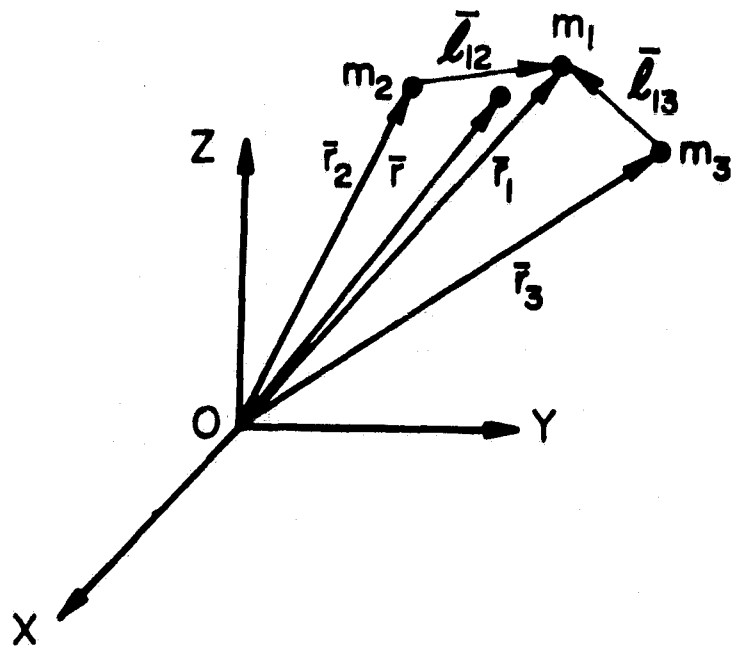

Fig. 1, The satellite relative to the center of the earth

The motion of the system will be described by six vector equations, three describing the linear displacement and three describing the angular motion of the satellite.

The first three equations are derived from Newton's law $\bar{F} = m\ddot{\bar{r}}$ and are:

$$\bar{F}_1+\bar{F}_{12}+\bar{F}_{13} = m_1\ddot{\bar{r}}_1 \qquad (1a)$$

$$F_2-F_{12} = m_2\ddot{\bar{r}}_2 \qquad (1b)$$

$$F_3-F_{13} = m_3\ddot{\bar{r}}_3 \qquad (1c)$$

The three equations describing the angular motion are derived from the equation:

$$\dot{\bar{H}} = \bar{M} \qquad \text{or}$$

$$\bar{\Phi}\cdot\dot{\bar{\omega}}\,\bar{\omega} \times \bar{\Phi}\cdot\bar{\omega} = \bar{M}$$

They are:

$$\overline{\Phi}_I \cdot \dot{\overline{\omega}}_I + \overline{\omega}_I \times \overline{\Phi}_I \cdot \overline{\omega}_I = \overline{T}_1 + \overline{T}_{12} + \overline{T}_{13} - \overline{r}_{12} \times \overline{F}_{12} - \overline{r}_{13} \times \overline{F}_{13} \quad (1d)$$

$$\overline{\Phi}_{II} \cdot \dot{\overline{\omega}}_{II} + \overline{\omega}_{II} \times \overline{\Phi}_I \cdot \overline{\omega}_{II} = \overline{T}_2 - \overline{T}_{12} \quad (1e)$$

$$\overline{\Phi}_{III} \cdot \dot{\overline{\omega}}_{III} + \overline{\omega}_{III} \times \overline{\Phi}_{III} \cdot \overline{\omega}_{III} = \overline{T}_3 - \overline{T}_{13} \quad (1f)$$

Where the notation used is as follows:

$\overline{F}_{1i}$ = reactive force transmitted on m_1 by m_i through hinge at m_i (i=2, 3)

$\overline{T}_{1i}$ = reactive torque transmitted on m_1 by m_i through hinge at m_i (i=2, 3)

$\overline{F}_i$ = resultant force on m_i, exclusive of reactive forces (i=1, 2, 3)

$\overline{T}_i$ = resultant force on m_i, exclusive of reactive torques (i=1, 2, 3)

$\overline{H}$ = angular momentum

$\overline{M}$ = moments

$\overline{\omega}_I$, $\overline{\omega}_{II}$, $\overline{\omega}_{III}$ = angular velocities of m_1, m_2, m_3 respectively

$\overline{\Phi}_I$, $\overline{\Phi}_{II}$, $\overline{\Phi}_{III}$ = moments of inertia dyadics of m_1, m_2, m_3 respectively

The location of the center of mass of the system is given by:

$$m_1\overline{r}_1 + m_2\overline{r}_2 + m_3\overline{r}_3 = m\,\overline{r} \quad (2)$$

Where

$$m = m_1 + m_2 + m_3 \quad (3)$$

Addition of (1a) through (1c) gives:

$$\overline{F}_1 + \overline{F}_2 + \overline{F}_3 = m_1\ddot{\overline{r}}_1 + m_2\ddot{\overline{r}}_2 + m_3\ddot{\overline{r}}_3$$

or, since the masses are constant with time:

$$\overline{F}_1 + \overline{F}_2 + \overline{F}_3 = m\,\ddot{\overline{r}} \quad (4)$$

Summation of moments about the center of mass of the system yield the following expression:

$$(\bar{r} - \bar{r}_1)\, m_1 + (\bar{r} - \bar{r}_2)\, m_2 + (\bar{r} - \bar{r}_3)\, m_3 = 0 \tag{6a}$$

From the geometry of Fig. 1:

$$\bar{r} - \bar{r}_2 = \bar{r} - \bar{r}_1 + \bar{l}_{12} \tag{6b}$$

$$\bar{r} - \bar{r}_3 = \bar{r} - \bar{r}_1 + \bar{l}_{13} \tag{6c}$$

From these last three equations, r_1, r_2 and r_3 are expressed in terms of $\bar{r}$, $\bar{l}_{12}$, $\bar{l}_{13}$ and the masses:

$$\bar{r}_1 = \bar{r} + \frac{m_2}{m}\,\bar{l}_{12} + \frac{m_3}{m}\,\bar{l}_{13} \tag{7a}$$

$$\bar{r}_2 = \bar{r} - \frac{m_1}{m}\,\bar{l}_{12} - \frac{m_3}{m}(\bar{l}_{12} - \bar{l}_{13}) \tag{7b}$$

$$r_3 = r - \frac{m_1}{m}\,l_{13} - \frac{m_2}{m}\,(\bar{l}_{13} - \bar{l}_{12}) \tag{7c}$$

From (1b), (1c), (4), (7b), and (7c) the following expressions for $\bar{F}_{12}$ and $\bar{F}_{13}$ are obtained:

$$\bar{F}_{12} = \frac{m_1 + m_3}{m}\,\bar{F}_2 - \frac{m_2}{m}\,(\bar{F}_1 + \bar{F}_3) + \left\{\frac{m_1+m_2}{m}\,\ddot{\bar{l}}_{12} + \frac{m_2 m_3}{m}\,(\ddot{\bar{l}}_{12} - \ddot{\bar{l}}_{13})\right\} \tag{8a}$$

$$\bar{F}_{13} = \frac{m_1+m_2}{m}\,\bar{F}_3 - \frac{m_3}{m}\,(\bar{F}_1 + \bar{F}_2) + \left\{\frac{m_1 m_3}{m}\,\ddot{\bar{l}}_{13} + \frac{m_2 m_3}{m}\,(\ddot{\bar{l}}_{13} - \ddot{\bar{l}}_{12})\right\} \tag{8b}$$

Noting that

$$\dot{\bar{l}}_{12} = \bar{\omega}_I \times \bar{l}_{12} \tag{9a}$$

and $\dot{\bar{I}}_{13} = \bar{\omega}_I \times \bar{I}_{13}$, (9b)

substituting (8a) and (8b) in (1d) will yield:

$$\bar{A}_1 + \bar{\Phi}_I \cdot \dot{\bar{\omega}}_I + \bar{\omega}_I \times \bar{\Phi}_I \cdot \bar{\omega}_I = \bar{T}_1 + \bar{T}_{12} + \bar{T}_{13}\,\bar{\bar{1}}_{12} \times \left[\bar{F}_2 - \frac{m_2}{m}(\bar{F}_1 + \bar{F}_2 + \bar{F}_3)\right] - 1_{13} \times \left[\bar{F}_3 - \frac{m_3}{m}(\bar{F}_1 + \bar{F}_2 + \bar{F}_3)\right] \quad (10)$$

where

$$A_1 = \frac{m_2}{m}\left[(m_1 + m_3)\,\bar{T}_{12} \times \ddot{\bar{T}}_{12} - m_3 \bar{T}_{12} \times \ddot{\bar{T}}_{13}\right] + \frac{m_3}{m}\left[(m_1 + m_2)\,\bar{T}_{13} \times \ddot{\bar{T}}_{13} - m_2 \bar{1}_{13} \times \ddot{\bar{1}}_{12}\right] \quad (11a)$$

Using equations (9) to obtain $\ddot{\bar{I}}_{12}$ and $\ddot{\bar{I}}_{13}$, and substituting these results in (11a), an equivalent expression for $\bar{A}_1$ is obtained:

$$\bar{A}_1 = \bar{A}_2 \cdot \dot{\bar{\omega}}_I + \bar{\omega}_I \times \bar{A}_2 \cdot \bar{\omega}_I \quad (11b)$$

Where

$$\bar{A}_2 = \frac{m_1 m_2}{m}(1^2_{12}\bar{I} - \bar{1}_{12}\bar{1}_{12}) + \frac{m_1 m_3}{m}(1^2_{13}\bar{I} - \bar{1}_{13}\bar{1}_{13}) + \frac{m_2 m_3}{m}\Big\{(1^2_{12}\bar{I} - \bar{1}_{12}\bar{1}_{12}) + (1^2_{13}\bar{I} - \bar{1}_{13}\bar{1}_{13} - 2(\bar{I}_{12} \cdot \bar{I}_{13})\,I + \bar{I}_{12}\bar{I}_{13} + \bar{I}_{13}\bar{I}_{12}\Big\} \quad (12)$$

and $\bar{I}$ is the idemfactor.

Using (11b), left side of (10) becomes:

$$(\Phi_I + \bar{A}_2) \cdot \dot{\bar{\omega}}_I + \bar{\omega}_I \times (\bar{\Phi}_I + \bar{A}_2) \cdot \bar{\omega}_I$$

Let

$$\bar{\Phi}'_I = \bar{\Phi}_I + \bar{A}_2 \quad (13)$$

then, rewriting (1e) and (1f) as they are, the three equations of angular motion will be:

$$\overline{\Phi}_I' \cdot \dot{\overline{\omega}}_I + \overline{\omega}_I \times \overline{\Phi}_I' \cdot \overline{\omega}_I = \overline{T}_1 + \overline{T}_{12} + \overline{T}_{13} - \overline{1}_{12} \times \left[\overline{F}_2 - \frac{m_2}{m} (\overline{F}_1 + \overline{F}_2 + \overline{F}_3)\right]$$

$$- \overline{1}_{13} \times \left[\overline{F}_3 - \frac{m_3}{m} (\overline{F}_1 - \overline{F}_2 + \overline{F}_3)\right] \qquad (14a)$$

$$\overline{\Phi}_{II} \cdot \dot{\overline{\omega}}_{II} + \overline{\omega}_{II} \times \overline{\Phi}_{II} \cdot \overline{\omega}_{II} = \overline{T}_2 - \overline{T}_{12} \qquad (14b)$$

$$\Phi_{III} \cdot \dot{\overline{\omega}}_{III} + \overline{\omega}_{III} \times \overline{\Phi}_{III} \cdot \overline{\omega}_{III} = \overline{T}_3 - \overline{T}_{13} \qquad (14c)$$

Note that $\overline{A}_1$, $\overline{A}_2$, and the $\overline{\Phi}$'s are all dyadics while the remaining terms in the equations are vectors, with the exception of the masses which are scalar quantities.

2. Gravitational forces and torques

Let:

$$\overline{T}_i = \overline{T}_i' + \overline{T}_{Gi} \qquad (15a)$$

and $$\overline{F}_i = \overline{F}_i' + \overline{F}_{Gi} \qquad (i = 1, 2, 3) \qquad (15b)$$

where $\overline{T}_{Gi}$ and $\overline{F}_{Gi}$ are gravitational torques and forces respectively and $\overline{T}_i'$ and $\overline{F}_i'$ are the external torques and forces acting on the satellite exclusive of those caused by gravity. Assuming a radially symmetric gravitational field (Ref. 2):

$$F_{Gi} = - \frac{\mu m_i \overline{r}_i}{r_i^3} \qquad (16a)$$

and $$T_{Gi} = \frac{3\mu}{r^3} \hat{r} \times \overline{\Phi}_i \cdot \hat{r} \qquad (i = 1, 2, 3) \qquad (16b)$$

where $\mu = g_o R^2$

g_o = gravity at the surface of the earth

R = radius of the earth

$\hat{\ }$ = symbol denoting a unit vector.

From (16a) it may easily be shown that

$$\sum_{i=1}^{3} \overline{F}_{Gi} = -\left(\frac{\mu}{r^3}\right) m\overline{r}$$

From (4) and (15b)

$$\sum_{i=1}^{3} (\overline{F}_1'' + \overline{F}_{Gi}) = m\ddot{\overline{r}}$$

If $\overline{F}_i' = 0$, i.e.: only gravitational forces act on satellite (other than reactive forces):

$$\ddot{\overline{r}} = -\frac{\mu\,\overline{r}}{r^3}$$

which is the equation of an eliptical orbit whose plane is fixed in space.

Using equations (7), (15) and (16), equation (14) may be rewritten as follows:

$$\overline{\Phi}_I' \cdot \dot{\overline{\omega}}_I + \overline{\omega}_I \times \overline{\Phi}_I' \cdot \overline{\omega}_I = \frac{3\mu}{3} \hat{r} \times \overline{\Phi}_I' \cdot \hat{r} + \overline{T}_1' + \overline{T}_{12} + \overline{T}_{13}$$

$$- \overline{I}_{12} \times \left[\overline{F}_2' - \frac{m_2}{m} (\overline{F}_1' + \overline{F}_2' + \overline{F}_3')\right]$$

$$- \overline{I}_{13} \times \left[\overline{F}_3' \frac{m_3}{m} (\overline{F}_1' + \overline{F}_2' + \overline{F}_3')\right] \qquad (17a)$$

$$\overline{\Phi}_{II} \cdot \dot{\overline{\omega}}_{II} + \overline{\omega}_{II} \times \overline{\Phi}_{II} \cdot \overline{\omega}_{II} = \frac{3\mu}{r^3} \hat{r} \times \overline{\Phi}_{II} \cdot \hat{r} + \overline{T}_2' - \overline{T}_{12} \qquad (17b)$$

$$\overline{\Phi}_{III} \cdot \dot{\overline{\omega}}_{III} + \overline{\omega}_{III} \times \overline{\Phi}_{III} \cdot \overline{\omega}_{III} = \frac{3\mu}{r^3} \hat{r} \times \overline{\Phi}_{III} \cdot \hat{r} + \overline{T}_3' - \overline{T}_{13} \qquad (17c)$$

3. Coordinate Systems.

Five orthogonal right handed reference frames will be used to describe the motion of the satellite.

i) An earth fixed reference frame (x y z) with origin at the center of the earth, the z-axis going through perigee and the y-axis in the direction of angular momentum. (Fig. 2) x z is the orbital plane.

ii) A rotating frame (x y z) with origin at the satellite center of mass, the z-axis always pointing away from the center of the earth and the

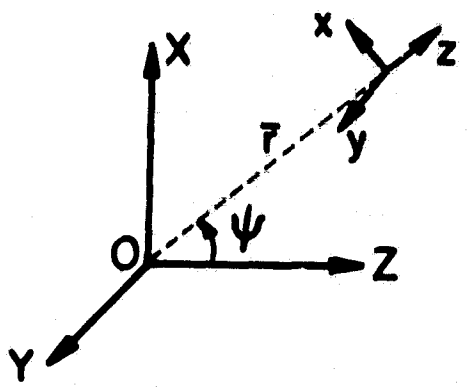

Fig. 2, Space coordinate systems

iii) A satellite fixed frame $(x_1 y_1 z_1)$ centered at m_1 and axis in the direction of the principal axis of inertia of the system. This reference frame is related to the x y z system by the following matrix (Ref. 2)

$$\begin{bmatrix} \hat{x}_1 \\ \hat{y}_1 \\ \hat{z}_1 \end{bmatrix} = n_{ij} \begin{bmatrix} \hat{x} \\ \hat{y} \\ \hat{z} \end{bmatrix} \qquad i=1, 2, 3 \qquad j=1, 2, 3 \qquad (18a)$$

where:

$$\left[n_{ij}\right] = \begin{bmatrix} \zeta^2 - \eta^2 - \varphi^2 + \chi^2 & 2(\zeta\eta + \varphi\chi) & 2(\zeta\varphi - \eta\chi) \\ 2(\zeta\eta - \varphi\chi) & -\zeta^2 + \eta^2 - \varphi^2 + \chi^2 & 2(\zeta\chi + \eta\varphi) \\ 2(\zeta\varphi + \eta\chi) & 2(\eta\varphi - \zeta\chi) & -\zeta^2 - \eta^2 + \varphi^2 + \chi^2 \end{bmatrix} \quad (18$$

and ζ, η, φ, and χ are Euler parameters (Ref. 5).

iv) The fourth and fifth reference frames ($x_2y_2z_2$ and $x_3y_3z_3$) will be fixed to m_2 and m_3 respectively (Fig. 3). It will be assumed that the only motion that m_2 and m_3 can have relative to m_1 is a rotation about the z_2 or z_3 axis respectively, i.e. the rods are assumed rigid, but hinges at m_2 and m_3 allow for rotation of the masses about the z_2 and z_3 axis. This motion will be restrained by torsional springs simulating the torsional elasticity of the actual rods.

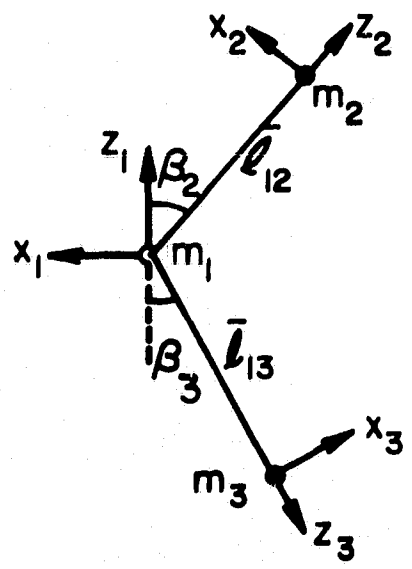

Fig. 3, Satellite - fixed frames

Let α_2 and α_3 be the angular displacements of m_2 and m_3 about z_2 and z_3 respectively, and β_2 and β_3 the swept back angles of the rods as indicated in Fig. 3, ; then the $x_i y_i z_i$ (i = 1, 2, 3) systems will be related as follows:

$$\begin{bmatrix} \hat{x}_2 \\ \hat{y}_2 \\ \hat{z}_2 \end{bmatrix} = \begin{bmatrix} \cos\alpha_2 \cos\beta_2 & \sin\alpha_2 & \cos\alpha_2 \sin\beta_2 \\ -\sin\alpha_2 \cos\beta_2 & \cos\alpha_2 & -\sin\alpha_2 \sin\beta_2 \\ -\sin\beta_2 & 0 & \cos\beta_2 \end{bmatrix} \begin{bmatrix} \hat{x}_1 \\ \hat{y}_1 \\ \hat{z}_1 \end{bmatrix} \tag{19a}$$

and

$$\begin{bmatrix} \hat{x}_3 \\ \hat{y}_3 \\ \hat{z}_3 \end{bmatrix} = \begin{bmatrix} -\cos\alpha_3 \cos\beta_3 & \sin\alpha_3 & \cos\alpha_3 \sin\beta_3 \\ \cos\beta_3 \sin\alpha_3 & \cos\alpha_3 & -\sin\alpha_3 \sin\beta_3 \\ \sin\beta_3 & 0 & -\cos\beta_3 \end{bmatrix} \begin{bmatrix} \hat{x}_1 \\ \hat{y}_1 \\ \hat{z}_1 \end{bmatrix} \tag{19b}$$

Note that α_2 and α_3 are dynamic parameters, but β_2 and β_3, due to the assumption that rods are rigid, are fixed for any given configuration. From Fig. 3, the following expressions for $\overline{T}_{12}$ and $\overline{T}_{13}$ are obtained:

$$\overline{\ell}_{12} = (\sin\beta_2 \hat{x}_1 - \cos\beta_2 \hat{z}_1)\, \ell_{12} \tag{20a}$$

$$\overline{\ell}_{13} = (\sin\beta_3 \hat{x}_1 + \cos\beta_3 \hat{z}_1)\, \ell_{13} \tag{20b}$$

4. Components of the angular equations of motion.

Equations (17) describe the angular motion of the satellite about its center of mass. The components of these equations about each axis of their corresponding coordinate system must be obtained before an explicit solution can be obtained. This is accomplished by obtaining each of the following scalar products:

Equation (17a) . $(\hat{x}_1, \hat{y}_1, \hat{z}_1)$

Equation (17b) . $(\hat{x}_2, \hat{y}_2, \hat{z}_2)$

Equation (17c) . $(\hat{x}_3, \hat{y}_3, \hat{z}_3)$

The task is somewhat simplified by the fact that equations (17) are all of the same general form with (17a) being the most involved due to the term $\overline{\Phi}_I'$. Thus, if the components of (17a) are obtained, those of (17b) and (17c) can easily be derived by analogy.

4a. Dyadic expressions.

Let the components of the angular velocities be given by:

$$\overline{\omega}_I = \omega_1 \hat{x}_2 + \omega_2 \hat{y}_3 + \omega_3 \hat{z}_1 \qquad (21a)$$

$$\overline{\omega}_{II} = \omega_4 \hat{x}_2 + \omega_5 \hat{y}_2 + \omega_6 \hat{z}_2 \qquad (21b)$$

$$\overline{\omega}_{III} = \omega_7 \hat{x}_3 + \omega_8 \hat{y}_3 + \omega_9 \hat{z}_3 \qquad (21c)$$

To simplify the equations to be derived, the problem may be specialized by assuming that:

i) $\beta_2 = \beta_3 \triangleq \beta$

ii) $m_2 = m_3 \triangleq m_D$

iii) m_1 and m_D are perfect spheres with moments of inertia I_s and I_D respectively, so that the following relations will hold:

$$\bar{\Phi}_I \cdot \hat{x}_1 = \Phi_I \cdot \hat{y}_1 = \bar{\Phi}_I \cdot \hat{z}_1 = I_s \bar{I} \tag{22a}$$

$$\bar{\Phi}_{II} \cdot \hat{x}_2 = \bar{\Phi}_{II} \cdot \hat{y}_2 = \bar{\Phi}_{II} \cdot \hat{z}_2 = \bar{\Phi}_{III} \cdot \hat{x}_3 = \bar{\Phi}_{III} \cdot \hat{y}_3 = \bar{\Phi}_{III} \cdot \hat{z}_3 = I_D \bar{I} \tag{22b}$$

Expanding (17a) one term at the time the following expressions are derived:

$$\bar{\Phi}'_1 \cdot \bar{\omega}_I = \bar{\Phi}_I \cdot (\dot{\omega}_1 \hat{x}_1 + \dot{\omega}_2 \hat{y}_1 + \dot{\omega}_3 \hat{z}_1) =$$

$$= \dot{\omega}_1 \bar{\Phi}'_I \cdot \hat{x}_1 + \dot{\omega}_2 \bar{\Phi}'_I \hat{y}_1 + \dot{\omega}_3 \bar{\Phi}'_I \cdot \hat{z}_1 \tag{23}$$

From (12) and (13) with $\bar{I}_{12}$ and $\bar{I}_{13}$ given by equations (20) the following results are obtained:

$$\bar{\Phi}'_I \cdot \hat{x}_1 = I_1 \hat{x}_2 + I_4 \hat{z}_1 \tag{24a}$$

$$\bar{\Phi}'_I \cdot \hat{y}_1 = I_2 \hat{y}_1 \tag{24b}$$

$$\bar{\Phi}'_I \cdot \hat{z}_1 = I_3 \hat{z}_1 + I_4 \hat{x}_1 \tag{24c}$$

where:

$$I_1 = (\bar{\Phi}'_I \cdot \hat{x}_1) \cdot \hat{x}_1 = I_s + \frac{m_D \cos^2 \beta}{m} \left[m_1 (1_{12}^2 + 1_{13}^2) + m_D (1_{12} + 1_{13})^2 \right] \tag{25a}$$

$$I_2 = (\bar{\Phi}'_I \cdot \hat{y}_1) \cdot \hat{y}_1 = I_s + \frac{m_D}{m} \left[m_1 (1_{12}^2 + 1_{13}^2) + m_D (1_{12} + 1_{13})^2 - 4 m_D I_{12} I_{13} \sin^2 \beta \right] \tag{25b}$$

$$I_3 = (\bar{\Phi}'_I \cdot \hat{z}_1) \cdot \hat{z}_1 = I_s + \frac{m_D \sin^2 \beta}{m} \left[m_1 (1_{12}^2 + 1_{13}^2) + m_D (1_{12} - 1_{13})^2 \right] \tag{25c}$$

$$I_4 = (\bar{\Phi}'_I \cdot \hat{x}_1) \cdot \hat{z}_1 = (\bar{\Phi}'_I \cdot \hat{z}_1) \cdot x_1 = \sin\beta \cos\beta (1_{12}^2 - 1_{13}^2) \frac{m_D (m_1 + m_D)}{m} \tag{25d}$$

I_4 is a term arising from the fact that $\beta \neq 0$. For the special case of $\beta = 0$, I_4 vanishes and as a result

$$I_1 = I_2 \text{ and } I_3 = I_s$$

Substituting equations (24) into (23):

$$\bar{\Phi}'_I \cdot \bar{\omega}_I = (\dot{\omega}_1 I_1 + \dot{\omega}_3 I_4) \hat{x}_1 + \dot{\omega}_2 I_2 \hat{y}_1 + (\dot{\omega}_3 I_3 + \dot{\omega}_1 I_4) \hat{z}_1 \tag{26a}$$

It logically follows that:

$$\bar{\Phi}_{II} \cdot \dot{\bar{\omega}}_{II} = I_D \dot{\bar{\omega}}_{II} \tag{26b}$$

and

$$\bar{\Phi}_{III} \dot{\bar{\omega}}_{III} = I_D \dot{\bar{\omega}}_{III} \tag{26c}$$

where I_D is as defined by (22b)

Following an analogous derivation:

$$\bar{\Phi}'_I \cdot \bar{\omega}_I = (\omega_1 I_1 + \omega_3 I_4)\hat{x}_1 + \omega_2 I_2 \hat{y}_1 + (\omega_3 I_3 + \omega_1 I_4)\hat{z}_1 \tag{27a}$$

$$\dot{\bar{\Phi}}_{II} \bar{\omega}_{II} = I_D \bar{\omega}_{II} \tag{27b}$$

$$\bar{\Phi}_{III} \cdot \bar{\omega}_{III} = I_D \bar{\omega}_{III} \tag{27c}$$

from which the following relations are easily obtained:

$$\bar{\omega}_I x \bar{\Phi}_I : \bar{\omega}_I = \left[\omega_2\omega_3(I_3 - I_2) + \omega_1\omega_2 I_4\right]\hat{x}_1 + \left[\omega_2\omega_3(I_1 - I_3) + \omega_3^2 - \omega_1^2) I_4\right]\hat{y}_1 + \left[\omega_1\omega_2(I_2 - I_1) - \omega_2\omega_3 I_4\right]\hat{z}_1 \tag{28a}$$

$$\bar{\omega}_i x \bar{\Phi}_i \cdot \bar{\omega}_i = 0 \qquad i = I, II \tag{28b}$$

From the definition of the coordinate systems:

$$\hat{r} = \hat{z} = n_{13}\hat{x}_1 + n_{23}\hat{y}_1 + n_{33}\hat{z}_1 \tag{29}$$

and by analogy to equations (28):

$$\hat{r} x \bar{\Phi}'_I \cdot \hat{r} = \left[n_{23}n_{33}(I_3 - I_2) + n_{13}n_{23}I_4\right]\hat{x}_1 + \left[n_{13}n_{33}(I_1 - I_3) + (n_{33}^2 - n_{13}^2)I_4\right]\hat{y}_1 + \left[n_{13}n_{23}(I_2 - I_1) - n_{23}n_{33}I_4\right]\hat{z}_1 \tag{30a}$$

$$\hat{r} x \bar{\Phi}_{II} \cdot \hat{r} = \hat{r} x \bar{\Phi}_{III} \cdot \hat{r} = 0 \tag{30b}$$

4b. Torques and forces

$\overline{T_1}$ is the control torque caused by the interaction of the generated magnetic flux and the earth magnetic field. $\overline{T_2}$ and $\overline{T_3}$ are damping torques caused by the motion of the magnetically anchored dampers in m_2 and m_3 respectively. The components of these three vectors are defined by:

$$\overline{T_i}' = T_{xi}\hat{x}_i + T_{yi}\hat{y}_i + T_{zi}\hat{z}_i \qquad (i = 1, 2, 3) \qquad (31)$$

$\overline{T_{12}}$ and $\overline{T_{13}}$ are reactive torques composed by:

i) constraint torques arising from the assumed rigidity of the rods, and

ii) restoring torques arising from the assumed tensional flexibility about $\hat{z}_2$ and $\hat{z}_3$

thus

$$\overline{T_{1j}} = T_{cx_j}\hat{x}_j + T_{cy_j}\hat{y}_j + T_{r_j}\hat{z}_j \quad (j = 2, 3) \qquad (32)$$

where

T_{r_j} = restoring torque about z_j

T_{cx_j}, T_{cy_j} = constraint torques about x_j and y_j respectively.

Let:

$$\overline{F_R} = -\overline{\ell}_{12}x\left[\overline{F_2}' \frac{m_2}{m}(F_1' + F_2' + F_3')\right] - \overline{\ell}_{13}x\left[\overline{F_3}' - \frac{m_3}{m}(F_1' + F_2' + F_3')\right] \qquad (33)$$

and define its components by:

$$\overline{F_R} = F_{Rx_1}\hat{x}_1 + F_{ry_1}\hat{y}_1 + F_{Rz_1}\hat{z}_1 \qquad (34)$$

From the equations derived in sections 4a and 4b and using the proper coordinate transformations, equations (17) may be expanded into their components producing the following set of equations:

$$\dot{\omega}_1 = I_{M_M} \quad (A - I_4 B/I_1)$$

$$\dot{\omega}_2 = D_2 + (T_{cx2} \sin \alpha_2 + T_{cy2} \cos \alpha_2 + T_{cx3} \sin \alpha_3 = T_{cy3} \cos \alpha_3)/I_2$$

$$\dot{\omega}_3 = I_{M_M} (B - I_4 A/I_3)$$

$$\dot{\omega}_4 = (t_{x2} - t_{cx2})/I_D$$

$$\dot{\omega}_5 = (T_{y2} - T_{cy2})/I_D \qquad (35)$$

$$\dot{\omega}_6 = (T_{z2} - T_{r2})/I_D$$

$$\dot{\omega}_7 = (T_{x3} - T_{cx3})/I_D$$

$$\dot{\omega}_8 = (T_{y3} - T_{cy3})/I_D$$

$$\omega_9 = (T_{z3} - T_{r3})/I_D$$

where:

$$I_M = I_3 I_1 / (I_3 I_1 - I_4^2)$$

$$A = D_1 = (T_{cx2} \cos \alpha_2 - T_{cy2} \sin \alpha_2 - T_{cx3} \cos \alpha_3 + T_{cy3} \sin \alpha_3) \cos \beta / I_1$$

$$B = D_3 + (T_{cx2} \cos \alpha_2 - T_{cy2} \sin \alpha_2 + T_{cx3} \cos \alpha_3 - T_{cy3} \sin \alpha_3) \sin \beta / I_3$$

$$D_1 = \left[(I_2 - I_3)(\omega_2 \omega_3 - G n_{23} n_{33}) - I_4 (\omega_1 \omega_2 - G n_{13} n_{23}) = T_{x_1} + \right.$$

$$\left. + F_{Rx1} - (T_{r2} + T_{r3}) \sin \beta \right] / I_1$$

$$D_2 = \left[(I_3 - I_1)(\omega_1 \omega_3 - G n_{13} n_{33}) - I_4 \left(\omega_3^2 - \omega_1^2 - G (n_{33}^2 - n_{13}^2) + T_{y1} + F_{Ry1} \right] \right) / I_2$$

$$D_3 = \left[(I_1 - I_2)(\omega_1 \omega_2 - G n_{13} n_{23}) + I_4 (\omega_2 \omega_3 - G n_{23} n_{33}) + \right.$$

$$\left. + T_{z1} + F_{Rz1} + (T_{r2} - T_{r3}) \cos \beta \right] / I_3$$

and from the orbital equation $\ddot{\bar{r}} = -\mu \bar{r}/r^3$ previously derived:

$$G = 3\mu/r^3 = 3 \dot{\psi}^2 / (1 + e \cos \psi)$$

where

$$\dot{\psi} = \Omega (1+e \cos \psi)^2/(1-e^2)^{3/2}$$

and

Ω = 2 π / orbital period

e= orbital eccentricity

ψ = angle from positive z-axis to $\overline{r}$

The above equation for $\dot{\psi}$ will be integrated together with equations (35) to obtain ψ as a function of time, which is needed to compute the components of the earth magnetic dipole as a function of orbital position.

Before a solution to (35) is obtained, the following parameters will have to be defined explicitly:

restoring, constraint, damping and control torques, α_2, α_3 and $\overline{F}_R$.

4b1. Restoring torques.

It will be assumed that both T_{r1} and T_{r2} are caused by two equal torsional springs at m_1 and m_2 respectively, so that

$$T_{rj} = K \alpha_j \qquad (j=1, 2) \qquad (36)$$

where K is the spring constant of the torsional springs.

4b2. Constraint torques, α_2 and α_3

The angular velocities of the three masses are related by

$$\overline{\omega}_{II} = \overline{\omega}_I + \dot{\alpha}_2 \hat{z}_2$$
$$\overline{\omega}_{III} = \overline{\omega}_I + \dot{\alpha}_3 \hat{z}_3$$

from which the following six equations are derived:

$$\left.\begin{aligned} (\overline{\omega}_{II} - \overline{\omega}_I) \cdot \hat{x}_2 &= 0 \\ (\overline{\omega}_{II} - \overline{\omega}_I) \cdot \hat{y}_2 &= 0 \\ (\overline{\omega}_{III} - \overline{\omega}_I) \cdot \hat{x}_3 &= 0 \\ (\overline{\omega}_{III} - \overline{\omega}_I) \cdot \hat{y}_3 &= 0 \end{aligned}\right\} \qquad (37)$$

$$\left.\begin{aligned}(\bar{\omega}_{II}-\bar{\omega}_{I})\cdot\hat{z}_2 &= \dot{\alpha}_2\\ (\bar{\omega}_{III}-\bar{\omega}_{I})\cdot\hat{z}_3 &= \dot{\alpha}_3\end{aligned}\right\} \qquad (38)$$

Equations (37) are four linear constraint equations which allow an explicit solution for the four constraint torques T_{cx1}, T_{cy1}, T_{cx2} and T_{cy2}. Equations (38) are first order differential equations which are integrated to obtain α_2 and α_3 as a function of time.

4b3. Damping torques.

As it was described in the introduction, each of the two end masses m_2 and m_3 contains a magnetically anchored damper which is assumed to follow the earth magnetic flux lines without lag. These two magnets will therefore always be in motion relative to the viscous fluid and the outer shells which contain them, producing damping torques. Define $\bar{\omega}_{em}$ as the effective rotation of the earth magnetic field, relative to the xyz system, as seen by the orbiting satellite. Let $\bar{\omega}_{emI}$, $\bar{\omega}_{emII}$, and $\bar{\omega}_{emIII}$ be $\bar{\omega}_{em}$ referred to the $x_1y_1z_1$, $x_2y_2z_2$, and $x_3y_3z_3$ systems respectively.

Also:

$$\bar{\omega}_{emII} = \bar{\omega}_{em4}\hat{x}_2 + \omega_{em5}y_2 + \omega_{em6}\hat{z}_2$$

$$\bar{\omega}_{em_{III}} = \omega_{em7}x_3 + \omega_{em8}\hat{y}_3 + \omega_{em9}\hat{z}_3$$

Then, the damping torques will be given by the following equations:

$$T_{x2} = (\omega_{em4}-\omega_4)C^*_D \qquad T_{x3} = (\omega_{em7}-\omega_7)C^*_D$$

$$T_{y2} = (\omega_{em5}-\omega_5)C^*_D \qquad T_{y3} = (\omega_{em8}-\omega_8)C^*_D \qquad (39)$$

$$T_{z2} = (\omega_{em6}-\omega_6)C^*_D \qquad T_{z3} = (\omega_{em9}-\omega_9)C^*_D$$

Where C_D^* is the viscous damping coefficient and it is assumed equal for both dampers.

4b4. Drag forces.

The only external forces other than gravity that will be considered to be acting on the satellite, will be drag forces. It will be assumed that these forces will not alter the orbit and that the equation

$$\ddot{\bar{r}} = -\mu \bar{r}/r^3$$

still describes the orbital motion.

The eccentricity of the orbit will be considered in computing atmospheric density as a function of altitude, but its effect on the direction of the drag force, which will be assumed to always act in the $-\hat{x}$ direction, will be neglected.

Thus: $$\bar{F}_i = -f_i \hat{x} \quad i = 1, 2, 3 \tag{40}$$

where $$f_i = \tfrac{1}{2} C_D \rho V^2 A_i \qquad i = 1, 2, 3 \tag{41}$$

and C_D = drag coefficient

ρ = atmospheric density

V = orbital velocity

A_i = frontal area of m_i ($i = 1, 2, 3$)

From equations (20), (33), (40), (41), the proper coordinate transformations and noting that since $m_2 = m_3$, $A_2 = A_3$ and $f_2 = f_3$; the components of $\bar{F}_R$ may be written as follows:

$$\begin{aligned} F_{Rx1} &= n_{21}\cos\beta\,(1_{12}-1_{13})\left\{f_2(m-2m_D)-f_1 m_D\right\}/m \\ F_{Ry1} &= -n_{11}\cos\beta\,(1_{12}-1_{13})\left\{f_2(m-2m_D)-f_1 m_D\right\}/m \\ &\quad -n_{31}\sin\beta(1_{12}+1_{13})\left\{f_2(m-2m_D)-f_1 m_D\right\}/m \end{aligned} \tag{42}$$

$$F_{Rz1}=n_{21}\sin\beta(l_{12}+l_{13})\left\{f_2(m-2m_D)-f_1 m_D\right\}/m$$

and programmed for solution on high speed digital computers. (The equations derived to this point were nondimensionalized.) The earth's magnetic field was simulated by a dipole (section 5) and a few simple control laws to generate T_1' were studied. Some of the results obtained and the description of a control law used, are given in section 6.

5. The earth magnetic field.

The field of a dipole located at the center of the earth will be assumed to represent with sufficient accuracy the actual earth magnetic field. (Ref. 3) The orbit will arbitrarily be chosen such that the axis of the magnetic dipole is in the XY plane (Fig. 4) at an angle from the positive X-axis.

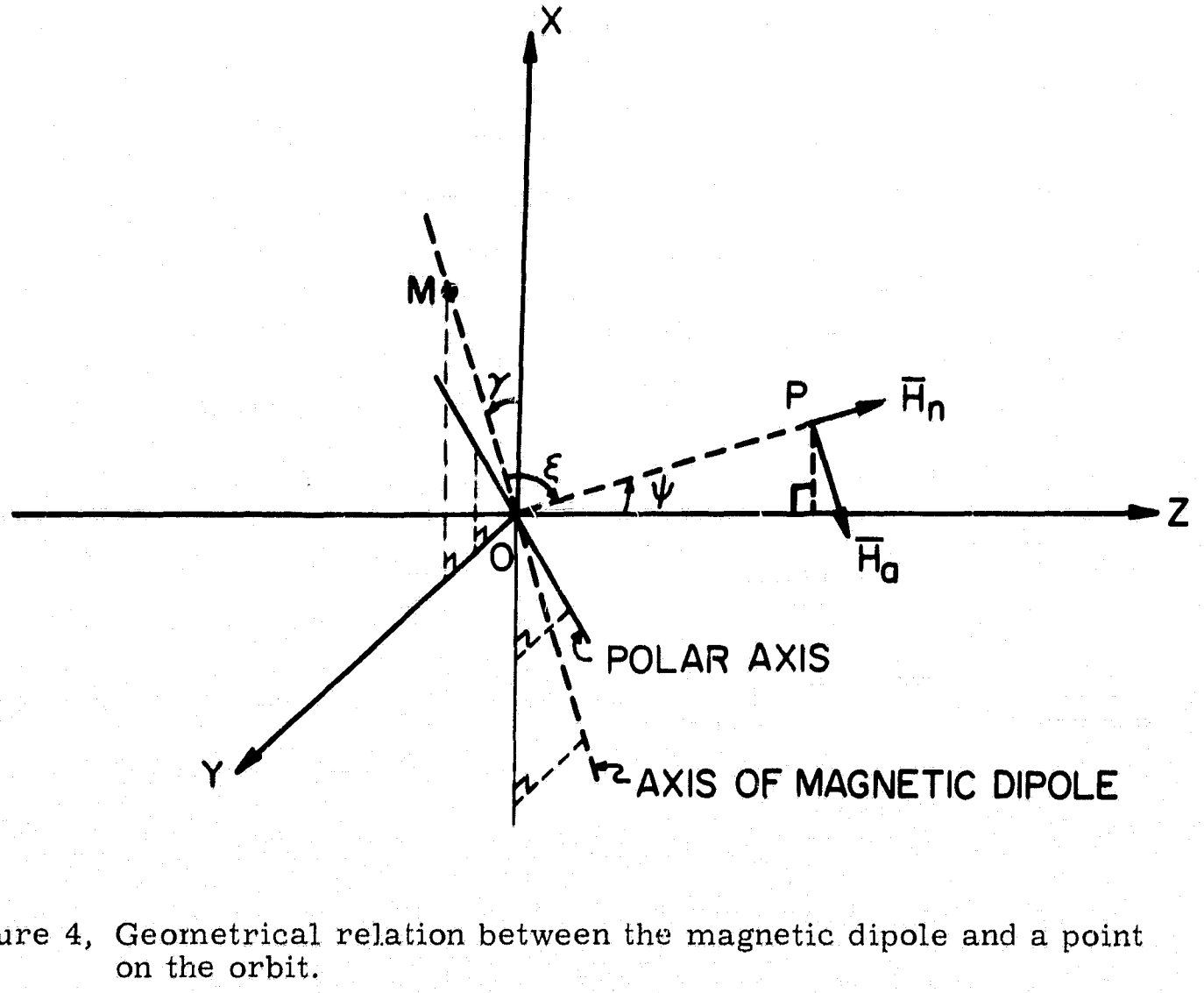

Figure 4, Geometrical relation between the magnetic dipole and a point on the orbit.

In figure 4, let $\overline{OP}$ define the position of the satellite at any given time, also let $\overline{OM}$ define an imaginary point on the magnetic axis and call ϵ the space angle formed by $\overline{OP}$ and $\overline{OM}$. Thus,. MOP; will define a plane containing the axial (H_a) and the normal (H_n) components of the total field ($\overline{H}$) created by the magnetic dipole, with H_a parallel to $\overline{OM}$ and H_n perpendicular to it. The magnitude of $\overline{H}_a$ and $\overline{H}_n$ is given by the following equations (Ref. 3)

$$H_a = .308\,(1-3\cos^2\gamma)\ /\ (r/r_e)^3 \qquad (43a)$$

$$H_n = .461\,\sin 2\gamma/\ (r/r_e)^3 \qquad (43b)$$

where $r = \left|\overline{OP}\right|$, r_e is the radius of the earth, and H_a and H_b are given in oersteds.

From geometrical relations defined by figure 4, the components of the magnetic dipole in the XYZ system are derived and are as given by the following expressions:

$$H_X = H_n (\sin \psi - \cos \epsilon \cos \gamma)/\sin \epsilon - H_a \cos \gamma \quad (44a)$$

$$H_y = -(H_a + H_n \cot \epsilon) \sin \gamma \quad (44b)$$

$$H_Z = H_n \cos \psi / \sin \epsilon \quad (44c)$$

The angle ϵ is given by $\epsilon = \text{arc} \cos (\sin \psi \cos \gamma)$ (45)

The rotation of the earth magnetic field as seen by the orbiting satellite is approximated by the following derivation:

define $\bar{H}_1 = \bar{H}$ at time t_1

$\bar{H}_2 = \bar{H}$ at time $t_2 (t_2 > t_1)$

and φ the angle between $\bar{H}_1$ and $\bar{H}_2$, then for small $(t_2 - t_1)$

$\omega_{em} \simeq \dfrac{\varphi}{t_2 - t_1}$ = rotation of the earth magnetic field as seen by the satellite.

The direction of the rotation will be perpendicular to the plane defined by $\bar{H}_1$ and $\bar{H}_2$. From the definition of a vector product, it follows that

$\dfrac{\bar{H}_1 x \bar{H}_2}{H_1 H_2 \sin \varphi}$ = a unit vector perpendicular to the plane defined by H_1 and H_2 (therefore parallel to ω_{em})

Thus

$$\bar{\omega}_{em} = \frac{\varphi \, H_1 x H_2}{H_1 H_2 \sin \varphi (t_2 - t_1)} \quad (46)$$

To obtain $\overline{\omega}_{em}$ referred to the xyz system, $\overline{H}_1$ and $\overline{H}_2$ in (46), will also have to be referred to the xyz system.

6. Control torques and results.

The torques that will be used to control the motion of the satellite on its orbit will arise from the interaction of the earth magnetic field and an induced field. The latter will be caused by a controllable current flowing through a set of three orthogonal coils wrapped around the main body of the satellite and therefore in the $x_1y_1z_1$ system.

It will be assumed that the number of turns and the area encircled are equal for each of the three coils, thus the only variable will be the current flowing through them.

The induced magnetic field vector will be given by

$$\overline{M}_F = N \overline{I}_c A \tag{47}$$

where

N = number of turns

A = area encircled

and

$$I_c = /I_c/ (a_1\hat{x}_1 + b_1\hat{y}_1 + c_1\hat{z}_1) \tag{48}$$

where I_c is the maximum current available a_1, b_1, c_1 represent the fraction of the total current flowing in the coil located in the plane perpendicular to x_1, y_1, z_1 respectively. The current can flow both counter and clockwise, thus the range of possible values for a_1, b_1, c_1 is in the interval -1 to +1.

From the equations derived in section 5, the components of the earth magnetic field relative to the $x_1y_1z_1$ system may be derived by simply using the proper transformation matrices. The result will be of the form

$$\overline{H}_1 = H_{x_1}\hat{x}_1 + H_{y_1}\hat{y}_1 + H_{z_1}\hat{z}_1 \tag{49}$$

The interaction of these two magnetic fields (induced (47) and earth (49) will produce a torque on the satellite whose magnitude and direction is given by the following vector product:

$$\bar{T} = \bar{M}_F x \bar{H}_1 \tag{50}$$

Substituting equations 47, 48, and 49 in 50 the following expression for the induced torque is obtained:

$$\bar{T} = NA\left|I_c\right| x \begin{bmatrix} x_1 & y_1 & z_1 \\ a_1 & b_1 & c_1 \\ H_{x_1} & H_{y_1} & H_{z_1} \end{bmatrix} \tag{51}$$

The problem which remains to be solved at this point is to determine a suitable control law that will define the desired values of a_1, b_1, and c_1 and therefore $\bar{\pi}$ as a function of time.

It obviously must be assumed that the earth magnetic field versus altitude and geographical position is known a priori and that its mathematical model is readily available for use in the necessary on-board calculations. The angular position and rates of the satellite on the orbit will be sensed by orientation sensing devices and therefore will be available for comparison to the a priori known desired position. This comparison will yield error signals which will be operated on by a control law yielding the values of a_1, b_1 and c_1 necessary to produce the induced torques that will correct the motion of the satellite.

This process is graphically described in Figure 5.

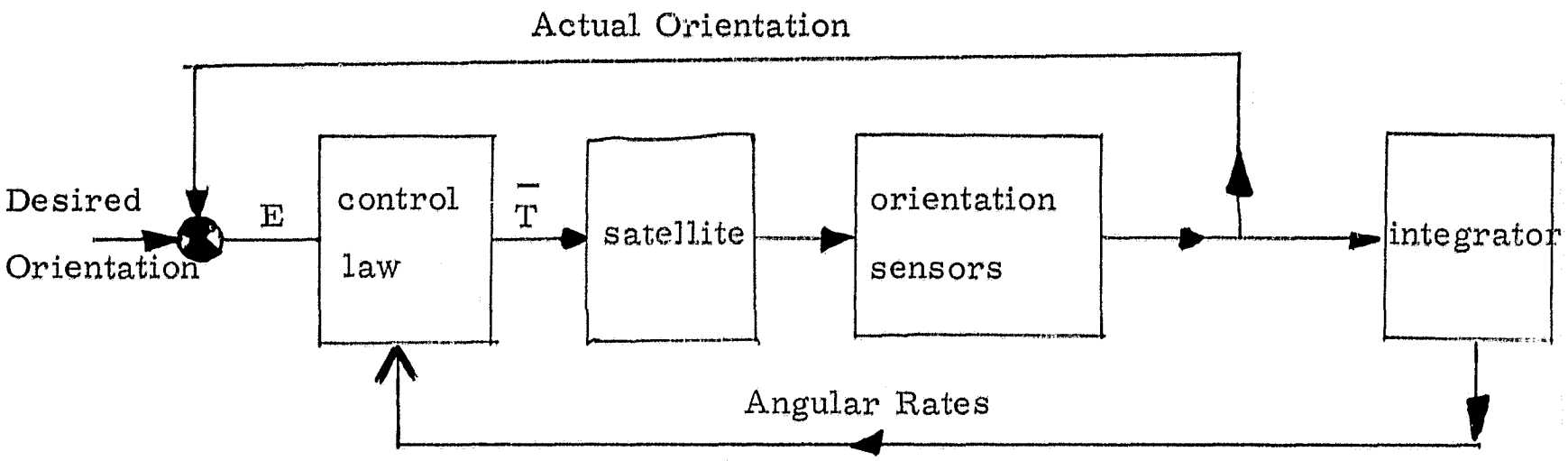

Figure 5. Box diagram of control loop.

From equation 51 it is apparent that for the special cases in which $\overline{H}_1$ is in the direction of one of the coordinate axis, only two components of torque may be generated. This will rarely happen, but the converse may cause a more severe problem, i. e.; during most of the orbiting time all three components of $\overline{H}_1$ will be non-zero, therefore with any one coil, at least two components of torque will be generated, one of which could be undesirable. Only two perpendicular coils are necessary to generate three components of torque, but a third coil, although not indispensable, will be used to afford better optimization capabilities. At this time, only a few simple control laws have been studied. More complex and efficient laws can be devised bearing in mind that increasing complexity increases the amount of computing equipment necessary to handle the problem. Thus onboard computer capabilities could be a limiting factor on the complexity of the control law.

Figure 6 shows the results obtained when trying to rotate the satellite 180^{o} in yaw and maintain this orientation. The simulation was for a 525 km circular orbit. Control was obtained by using only two coils of one foot radius and 100 turns each. A current of one ampere is allowed to flow through them in either direction when so desired. Thus the possible values of a_1, b_1, and c_1 in equation 48 are:

$$A_1 = 0, \pm 1 \; ; b_1 = 0, \pm 1 \; ; c_1 = 0$$

and from equation 51:

$$\overline{T} = NA/I_c/ \begin{bmatrix} b_1 H_{z_1} \\ -a_1 H_{z_1} \\ a_1 H_{y_2} - b_1 H_{x_2} \end{bmatrix} \tag{52}$$

where $a_1 H_{y_2} - b_1 H_{x_2}$ is the yaw component of torque.

The simulation was initiated with the satellite stable in its orbit and with a yaw orientation of zero degrees (i. e. : flying into the stream). The following simple control logic was then used:

1) Positive torque in yaw is applied until yaw=110°.

2) For $100^{\circ} \leq$ yaw $\leq 177^{\circ}$ torque is applied only if the yaw angular velocity is under 0. 2 revs/orbit.

3) a) for yaw $> 177^{\circ}$ and decreasing, skip to steps 6 and 7.

b) for yaw $> 177^{\circ}$ and increasing, continue with step 4.

4) If yaw $> 180^{\circ}$ apply negative torque to reduce yaw rate and eventually reverse its direction.

5) If $177^{\circ} <$ yaw $\leq 180^{\circ}$ no torque is applied. (Steps 6, 7 and 8 are taken only if either 4 or 5 were not taken).

6) If yaw $< 180^{\circ}$ apply positive torque to reverse yaw rate and bring yaw back to 180°.

7) If $183^{\circ} \geq$ yaw $> 180^{\circ}$, no torque is applied.

8) If yaw $> 183^{\circ}$ apply negative torque to bring yaw to 180°.

Once this point in the logic has been reached, the desired sign of the torque in yaw is known; that is, the desired sign of $(a_1 H_{y_2} - b_1 H_{x_2})$ is known. Thus, since H_{x_1} and H_{y_2} are the a-priori known components of the earth magnetic

field, and are therefore non-controllable, a_1 and b_1 are selected to both yield the proper sign and maximize the magnitude of the torque in yaw. When doing this, the arising torques in pitch and roll are not considered introducing, as a consequence, undesired pitch and roll oscillations.

Conclusions.

The simulations conducted to this point indicate that the control scheme treated in this paper is feasible, but better control laws have to be tested. These laws must remain simple in order not to exceed the eventual on-board computer capabilities, but they must consider not only motion in yaw but also in pitch and roll when generating the control torques. Further study in this area will be conducted.

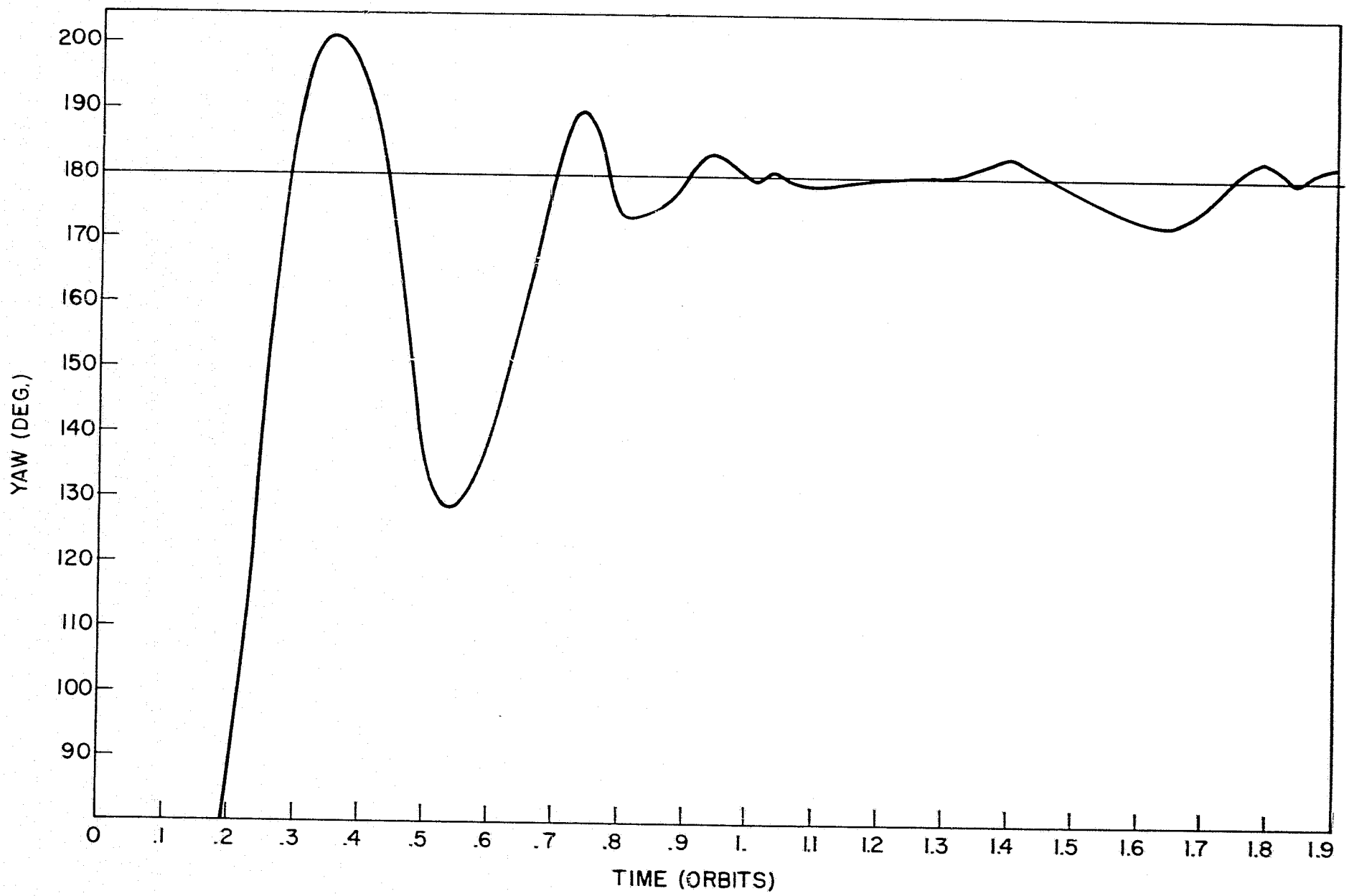

Figure 6. Temperature errors for configuration 2 using helium.

List of symbols.

1. English symbols.

A	Area encircled by coils.
A_1	As given by equation 11a
A_2	As given by equation 12
A_i	Frontal area of body i
C_D^*	Viscous damping constant
C_D	Drag coefficient
e	Orbital ecentricity
f_i	Drag force on body i
F_{Gi}	Gravitational force on body i
F_R	As given by equation 33
$F_{R_{x_1}}, F_{R_{y_i}}, F_{R_{z_1}}$	Components of $\bar{F}_R$ in the $x_1y_1z_1$ system
F_i	Resultant force on body i exclusive of reactive forces
F_i'	External force on body i exclusive of gravity forces
F_{12}	Reactive force (body 2)
F_{13}	Reactive force (body 3)
g_o	Acceleration of gravity on surface of earth
H	Earth magnetic field
H_a, H_n	Axial and normal components of $\bar{H}$
H_X, H_Y, H_Z	Components of $\bar{H}$ in the XYZ system
I_c	Maximum current available to generate flux
I_s	Moment of inertia of main body
I_1---I_4	"Equivalent moments of inertia" (equations 25)
K	Torsional spring constant of booms

l_{12}	Length of boom connecting bodies 1 and 2
l_{13}	Length of boom connecting bodies 1 and 3
m	Total mass of satellite
m_i	Mass of body i
m_D	Mass of dampers
$\overline{M}_F$	Induced magnetic field vector
n_{ij}	Direction cosines of x, y, z, with respect to xyz
N	Number of turns of coils
r	Distance from satellite to earth center
r_e	Radius of the earth
$\overline{r}_i$	Position vector of body i
$\overline{T}$	Controlling torque
T_i	Resultant torque on body i exclusive of reactive torques
T_i'	External torque on body i exclusive of gravity torques
T_{12}	Reactive torque (body 2)
T_{13}	Reactive torque (body 3)
T_{Gi}	Gravitational torque on body i
$T_{x_1}, T_{y_1}, T_{z_1}$	Components of magnetically induced torques
$T_{cx_2}, T_{cy_2}, T_{cx_3}, T_{cy_3}$	Constraint torques on bodies 2 and 3
T_{r_2}, T_{r_3}	Restoring torques on bodies 2 and 3
XYZ	Fixed frame coordinates
xyz	Rotating frame coordinates
$x_i y_i z_i$	Body i coordinates
V	Orbital velocity

2. Greek symbols.

α_2	Relative angle of rotation of body 2 about its rod
α_3	Relative angle of rotation of body 3 about its rod
β_2, β_3	Sweep back angles (see figure 3)
β	$\beta = \beta_2 - \beta_3$ when condition is satisfied
ϵ	Angle between $\overline{r}$ and magnetic axis
φ	Euler parameter
η	Euler parameter
μ	Gravitational constant
ξ	Euler parameter
ρ	Atmospheric density
Φ_i	Moment of inertia dyadic of body i
Φ_i'	Equivalent inertia dyadic of body 1 (Equation 13)
χ	Euler parameter
ψ	True anomaly of ellipse
Ω	Mean orbital angular speed
$\omega_I, \omega_{II}, \omega_{III}$	Angular velocities of bodies 1, 2, and 3 respectively
$\omega_1, \omega_2, \omega_3$	Components of ω_I in the x, y, z, system
$\omega_4, \omega_5, \omega_6$	Components of ω_{II} in the $x_2y_2z_2$ system
$\omega_7, \omega_8, \omega_9$	Components of ω_{III} in the $x_3y_3z_3$ system
ω_{em}	Relative rotation of earth magnetic field as seen by satellite
ω_{emI}	Components of $\overline{\omega}_{em}$ in the $x_1y_1z_1$ system
ω_{emII}	Components of $\overline{\omega}_{em}$ in the $x_2y_2z_2$ system
ω_{emIII}	Components of $\overline{\omega}_{em}$ in the $x_3y_3z_3$ system

References

1. Etkin, B., H. Maeda, Attitude Stability of Articulated Gravity Oriented Satellites, Parts I and II, UTIA Reports, 89 and 93, Nov. 1962 and June 1963.

2. Fletcher, H. J., L. Rongred, E. Y. Yu, Dynamics Analysis of a Two Body Gravitationally Oriented Satellite, Bell System Technical Jour., 2239-2266, September 1963.

3. Gerlach, O. H., Attitude Stabilization and Control of Earth Satellites, Space Science Review, No. 4, Vol. IV, 541-582, June 1965.

4. Roberson, R. E., Gravitational Torques on a Satellite Vehicle, Journal of Franklin Institute, No. 1, Vol. 265, 13-22, June 1958.

5. Whittaker, E. T., A Treatise on the Analytical Dynamics of Particles and Rigid Bodies, p. 8-16, Dover Publications, New York, 1944.

6. Zajac, E. E., Damping of a Gravitationally Oriented Two-Body Satellite, ARS Journal, No. 12, Vol. 32, 1871-1875, Dec. 1962.

7. All G. E. and U of M reports and proposals on MICHAEL.

Acknowledgment

The comments and suggestions of Professor D. T. Greenwood of the Aerospace Engineering Department of the University of Michigan were extremely valuable in the course of this work. His assistance in revising the original manuscript was also very helpful.